STATIC VERSUS DYNAMIC STRUCTURAL RESPONSE OF BRIDGE PIERS TO BARGE COLLISION LOADS

By

LONG HOANG BUI

A THESIS PRESENTED TO THE GRADUATE SCHOOL
OF THE UNIVERSITY OF FLORIDA IN PARTIAL FULFILLMENT
OF THE REQUIREMENTS FOR THE DEGREE OF
MASTER OF ENGINEERING

UNIVERSITY OF FLORIDA

2005

To my parents

ACKNOWLEDGMENTS

First of all, I would like to thank my advisor, Dr. Gary R. Consolazio for his invaluable guidance, great mentorship, encouragement and patience. His knowledge and expertise have brought me a great educational experience. This research would not have been possible without him.

I would like to thank Dr Michael McVay, whose contributions in this research have been tremendous. I clearly benefited from all the hours of interesting discussion with him.

I would like to thank Drs. H.R. Hamilton, and Kurtis R. Gurley for serving on my supervisory committee.

I also wish to extend my thanks to David Cowan for his contribution and support, and Dr. Jae Chung for his help and enthusiastic encouragement. A special note of appreciation goes to Scott Wasman for his experimental soil data.

Finally, I would like to thank my parents, my brother and my friends for all the love, support and encouragement they have for me.

TABLE OF CONTENTS

page

LIST OF TABLES

Table page

LIST OF FIGURES

Abstract of Thesis Presented to the Graduate School
of the University of Florida in Partial Fulfillment of the
Requirements for the Degree of Master of Engineering

STATIC VERSUS DYNAMIC STRUCTURAL RESPONSE OF BRIDGE PIERS TO BARGE COLLISION LOADS

By

Long Hoang Bui

December 2005

Chair: Gary R. Consolazio
Major Department: Civil and Coastal Engineering

Vessel collision design for bridges crossing navigable waterways is an important consideration since it significantly affects the total cost of bridges. Economical design requires appropriate determination of impact loads imparted to bridge piers. While the impact load is dynamic in nature, current provisions for bridge design are based on static approximations of structural behavior and limited experimental data. Dynamic barge impact load prediction using finite element analysis requires proper modeling of both barge and pier. Magnitude and period of impact loads are affected by numerous factors including mass, velocity, structural configuration of the barge; mass, stiffness, structural configuration of the piers; and the behavior of soil. This thesis presents an investigation of the soil responses, determination of resistance sources under static and dynamic impact loading conditions, and development of finite element models of pier structures using the LS-DYNA and FB-Multipier finite element analysis programs. Full-scale test data are used to calibrate the pier-soil finite element models so that they are capable of capturing

the relevant dynamic pier and soil effects. Static and dynamic contributions of the soil resistance on embedded pile caps are also incorporated into the models. Dynamic analysis results of the calibrated models such as time histories of pier displacement, soil forces on the cap and seal, pile shear and pile deflected shapes are compared with experimental results. Dynamic contributions of resistance from the soil and pier mass are quantified and discussed. Pier structural demand-capacity ratios from dynamic and static analyses are also computed and compared.

CHAPTER 1
INTRODUCTION

1.1 Motivations for Considering Barge Impact Loads

Bridges crossing coastal or inland waterways are susceptible to collapse caused by vessels impacting pier structures. The increase in vessel size and traffic density has put these bridges at higher risk of being hit (Saul and Svensson 1983). Direct inclusion of ship and barge impact loads on bridge structures was neglected in bridge design until about twenty-five years ago. The possibility of such a catastrophic collision was considered very small and therefore disregarded. Additionally, designing bridges to resist such an extreme event could be overly conservative and uneconomical. Moreover, methods for determining impact forces were not well understood or established.

Continued incidents of accidents due to the vessel collision with bridges has drawn special attention from bridge designers all over the world, thus introducing impact forces into the bridge design process. A severe accident, which became a major turning point in the development of vessel collision design criteria for bridges in the United States (American Association of State Highway and Transportation Officials [AASHTO] 1991), was the 1980 collapse of the Sunshine Skyway Bridge crossing Tampa Bay in Florida. The cargo ship Summit Venture rammed one of the support piers of the bridge destroying about 1300ft of bridge deck and causing the loss of thirty-five lives. Similarly devastating events have also occurred as the result of barge collisions. In 1993, a CSX railroad bridge over Bayou Canot near Mobile, Alabama, was hit by a barge tow resulting in derailment of an Amtrak train and the loss of forty-seven lives. On September 15, 2001, a four-barge

tow collided with the Queen Isabella causeway, the longest bridge in Texas and the only bridge leading to South Padre Island. The collision resulted in eight fatalities. Most recently, on May 26, 2002 the towboat Robert Y. Love, pushing two barges side by side, veered off course and collided with a pier of the Interstate 40 highway bridge near Webber's Falls, Oklahoma causing the collapse of 503-feet section of bridge into the Arkansas River. Fourteen people were killed and five others were injured.

In addition to fatalities, the consequences of such accidents involve large economic losses due to costs of repair or replacement as well as loss of transportation service. Accidents involving vessels impacting bridge piers occur worldwide at an approximate average of one serious collision per year. The importance of considering vessel collision loads in bridge design is thus clear.

The inclusion of barge impact loads in new designs, in bridge sufficiency ratings, and in rehabilitation and replacement prioritization of in-service structures requires acceptably accurate yet practical methods for determining barge impact loads and associated structural responses. Current bridge design practices for vessel impact loading in the United State follow the AASHTO provisions (AASHTO 1991, 1994), in which simplified procedures are given for determining static equivalent loads instead of requiring dynamic analysis. Moreover, present day bridges are also at risk of terrorist attacks and vulnerability assessment for scenarios involving intentional ramming, which would usually produce large dynamic impact forces, may warrant more sophisticated analysis procedures than would be justifiable in a typical bridge design.

1.2 Barge Collision Events

For bridges over navigable waterways, both superstructures and substructures are at risk of being hit by errant vessels. However, past accidents have shown that piers are the

most vulnerable elements to damage from vessel collisions. Due to the low vertical profile of barges, the impact point is typically on the pier column near the waterline. A common characteristic of most barge collisions is that the loads are transient, that is short duration in time. Furthermore, barge collision loadings on pier structures are usually very large in magnitude due to the relatively high velocity and the large mass associated with barges and their cargo. The variation in magnitude and duration of the load is dependent on factors such as the mass, velocity, structural type of the barge; the structural configuration, mass, stiffness of the piers and superstructure and the connection between them; and the properties of the soil surrounding the pier foundation. One of the most significant effects on the impact loads developed is the resistance and deformation behavior of the barge bow. Each type and size of barge has its own load-deformation curve. However, research has shown that the typical trend of the impact force is a rapid increase at small crush levels, followed by an abrupt leveling off of force due to buckling of internal frames and yielding of barge bow material. At higher deformation levels, the trend of the load may gradually increase due to geometric effects such as membrane action.

When a barge strikes a pier in the head-on manner, a portion of the momentum of the barge is transferred to the pier in the form of an impulsive force. A component of the barge impact energy is also absorbed through plastic deformation of the barge bow. During oblique impacts between *multi-barge* flotillas and bridge piers, not all of the momentum of the flotilla may transfer to the pier as the individual barges in the flotilla break away from each other. In such a case, the impact force caused by the flotilla is not related solely to the total momentum of the entire flotilla but also depends on the barge-

to-barge cable connection properties. Flexibility and breakup of the barge flotilla are functions of the lashings that tie the barges together. Moreover, flexibility within the flotilla allows energy absorption within the flotilla. Kinetic energy of the flotilla is not only dissipated through crushing of the barge bow impacting the pier but also through the buckling, crushing and friction among the barges and rotation of the barges in the flotilla.

1.3 Sources of Bridge Pier Resistance

Lateral loads on a bridge pier are ultimately transferred to the soil via a direct load path to the foundation of the impacted pier and an indirect load path through the superstructure to the adjacent piers. Available resistances of bridge piers against lateral loads, therefore, depend on structural as well as soil capacities. Depending on the nature of lateral loads, pier configuration and the connections between substructure and superstructure, various types of resistance may be mobilized.

If static lateral loads are applied to a pier, which has a pile cap above the ground level, pile shears of the impacted pier will carry most of the load while the superstructure will carry a lesser amount. If battered piles are used, pile axial forces also participate in resisting the lateral loads. For a pier foundation with plumb piles, a fixed-head condition at the pile top will increase the lateral resistance capacity of the pier through increased flexural stiffness and through the development of pile axial forces that contribute resistance indirectly through frame action. For a cap-embedded pier, that is when the pile cap is buried below the ground level, the passive force of soil pressure on the cap and the skin friction forces developed on the soil cap surfaces also provide significant amounts of resistance against static lateral loads.

In addition to above resistances, under dynamic loading like barge impact, a variety of other sources of resistance can participate in resisting the load. When a barge impacts a

pier, a large inertial force of the pier mass is generated. Lateral soil reactions on the pile and pile cap may also increase significantly under dynamic loading due to load rate effects (rate dependent stiffness) in the soil. Furthermore, the superstructure contributes to the lateral resistance of the pier not only by shedding a portion of the load to the adjacent piers through stiffness (static resistance) but also through mass related inertial resistance.

While a considerable portion of lateral resistance associated with dynamic loading may be mobilized, static analysis fails to take into account of these resistances. Therefore the pier capacity against impact loads may be underestimated. This thesis focuses on quantifying the contribution of dynamic resistances of pier structures and the soil against impact loads. Finite element models of the pier and soil are developed and calibrated to represent the physical behavior the system. Severity of pier structures analyzed dynamically using measured impact loads is compared to cases analyzed statically using the equivalent static loads.

CHAPTER 2
NUMERICAL PIER ANALYSIS PROCEDURES

2.1 Introduction

An ultimate goal of bridge design against barge impact is preventing collapse of the superstructure that carries traffic. To achieve this goal, the load experienced by each bridge component must be limited such that the structure, as a whole, remains stable. To assess the resistance and response of pier elements, structural analysis for barge impact requires the determination of collision loads that are imparted to the pier. A common approach involves determining an equivalent static load using procedures given by AASHTO (1991, 1994). Such loads are then used to conduct a static analysis of the pier structure.

Since barge collision with pier is a dynamic event, the most accurate prediction of impact load and pier response requires an alternative, more refined procedure in which both high-resolution finite element barge and pier models are analyzed dynamically. This approach is typically computationally expensive and may not be practical for routine bride design since it requires significant time and effort. An alternative numerically efficient dynamic method developed by Consolazio et al. (2005) involves the use of low order barge model rather than a high-resolution model to dynamically analyze pier response. This method has shown promise as an alternative to the current code-specified static bridge analysis procedure. Unlike the static method, in which the impact load is determined before the analysis, in dynamic methods, the impact load is determined at each time step during the analysis process.

2.2 Static Analysis Procedure

Current design documents for barge impact load determination are the AASHTO Guide Specification and Commentary for Vessel Collision Design of Highway bridges (AASHTO 1991) and the AASHTO LRFD Bridge Design Specifications (AASHTO 1994). These documents have different methods for risk analysis; however, their procedures for calculating barge impact loads are the same. The purpose of the AASHTO provisions is to provide a simplified method for computing barge impact equivalent static loads for the design of new bridges and for the evaluation of existing bridges. The specifications apply to all bridge types crossing navigable shallow draft inland waterways with barge traffic.

Impact load calculation per AASHTO requires the collection of data relating to vessel traffic, vessel transit speeds, vessel loading characteristic, bridge geometry, waterway and navigable channel geometry, water depths and environmental conditions. Once the design impact speed and flotilla size (mass) have been established, impact kinetic energy is calculated as (AASHTO 1991):

$$KE = \frac{C_H W (V)^2}{29.2} \tag{2.1}$$

where KE is the barge kinetic energy (kip-ft), W is the vessel weigh (tonnes), C_H is a hydrodynamic mass coefficient and V is the vessel impact speed (ft/sec). Equation (2.1) is derived from the standard kinetic energy of a moving object:

$$KE = \frac{W (V)^2}{2g} \tag{2.2}$$

where g is the acceleration of gravity.

The hydrodynamic mass coefficient C_H is included in equation (2.1) to account for additional inertial force provided by the mass of water surrounding and moving with the vessel. Determination of C_H depends on many factors such as water depth, under-keel clearance, distances to obstacle, shape of the vessel, vessel speed, currents, position and direction of the vessel, and the cleanliness of the hull underwater. For a barge moving in a straight forward motion, AASHTO recommend the following values of C_H depending on under-keel clearance and draft:

- For large underkeel clearances $(\geq 0.5 \cdot Draft)$: $C_H = 1.05$
- For small underkeel clearances $(\leq 0.1 \cdot Draft)$: $C_H = 1.25$

where the under-keel clearance is the distance between the bottom of the vessel and the bottom of the waterway. C_H is estimated by interpolation for under-keel clearances between the two limits given above.

Based on the fact that a significant component of barge energy is dissipated through crushing of the barge bow, an empirical relationship between kinetic energy and crush depth is given by AASHTO (1991) as:

$$a_B = \left[\left[1 + \frac{KE}{5672}\right]^{1/2} - 1\right]\left[\frac{10.2}{R_B}\right] \tag{2.3}$$

where a_B is the barge bow crush depth (ft), KE is the barge collision energy (kip-ft) and $R_B = \left(B_B / 35\right)$ is the barge width modification factor, where B_B is the barge width (ft). The barge width modification factor is used to modify the impact forces for barges whose width is different than 35ft.

Once the crush depth is determined, the static-equivalent barge impact force is calculated as:

$$P_B = \begin{cases} (4112) a_B \cdot R_B & a_B < 0.34\, ft \\ (1349 + 110 \cdot a_B) \cdot R_B & a_B \geq 0.34\, ft \end{cases} \quad (2.4)$$

where P_B is the equivalent static impact force (kips) and a_B is the barge bow damage depth.

Since very little experimental research in the area of the barge collision impact forces has been reported and published, the AASHTO method of determining barge impact force was based only on the research conducted by Meir-Dornberg in 1983 (AASHTO 1991). Experimental tests and associated analytical modeling were performed for barge collisions with lock entrance structures and bridge piers to study the collision force and deformation of the barge bow. Meir-Dornberg's study involved numerical computations, dynamic loading with a pendulum hammer on three reduced-scale barge bottom models, and static loading on one reduced-scale barge bottom model of a standard European Barge, Type II. Empirical relationship equations were then developed that related kinetic energy, barge deformation and static-equivalent impact force. These equations were adopted by AASHTO and modified only to account for the deviation of average barge width in U.S. inland waterway system versus in Europe. In Figure 2.1 Equation 2.3 and 2.4 are combined to yield static-equivalent impact load as a function of initial impact energy.

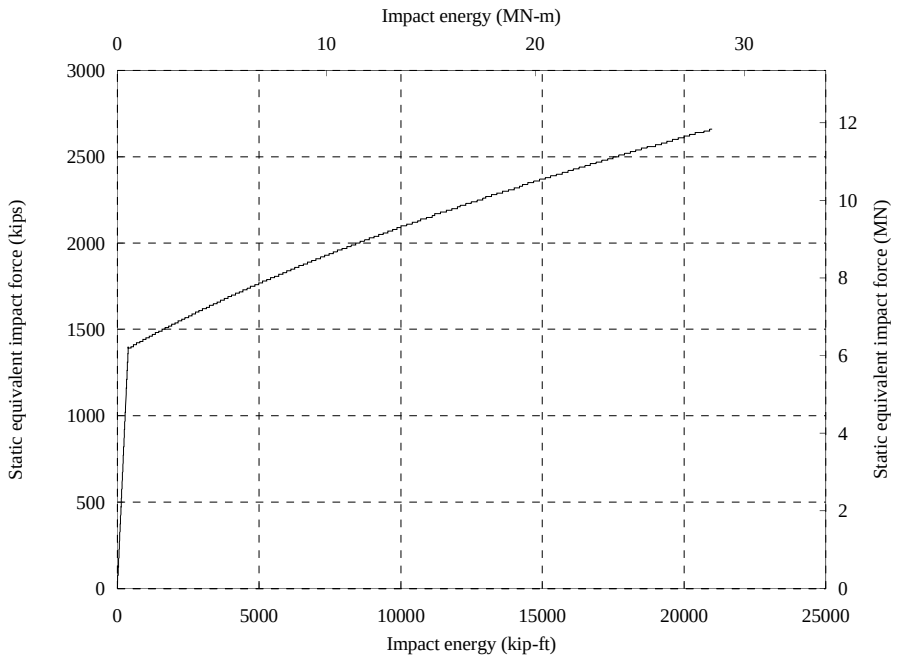

Figure 2.1 Impact force vs. impact energy relationship adopted by AASHTO

The equivalent static force computed via the AASHTO expression is then applied to a pier structure model to determine structural responses and check for overall stability and local strength of pier components using static analysis. Collision loads are usually very large in magnitude and thus significant deformations of structural components may occur. Therefore, the numerical pier model should be able to represent both geometric and material nonlinear behaviors. Material non-linearity is accounted for by specifying nonlinear stress-strain relationships for the material used in the pier. Additionally, one of the key factors that affects the accuracy of the computed structural response is the soil modeling techniques due to highly non-linear characteristics of the soil. Superstructure modeling may also be included if load shedding from an impacted pier to adjacent piers is to be taken into account. Proper representation of superstructure effects requires careful detailing of the pier-structure bearing connections.

2.3 Dynamic Analysis using FB-Multipier

Many dynamic structural analysis problems require the engineer/analyst to prescribe time-varying parameters such as load, displacement or time histories of ground acceleration. However, in some cases such parameters cannot be determined ahead of time. For dynamic pier analysis under barge impact, the impact load is a function of the structure and soil characteristics and is therefore unknown prior to analysis. Thus such load must be determined as part of the analysis. Previous work (Consolazio et al. 2005) has included a single degree of freedom (SDOF) barge being coupled to a multi degree of freedom (MDOF) pier analysis code, FB-Multipier (Florida BSI 2005). This combined program has the capability to analyze pier structures under barge impact without the need for prescribed time-varying loads. The key analysis technique used in this modified program is that the impact load is computed by coupling a low order (SDOF) barge model to the MDOF pier module (see Figure 2.2) through the shared impact force P_b. Important characteristics and behaviors of the multi-DOF barge model such as mass and nonlinear stiffness of the barge bow are represented by the SDOF barge model.

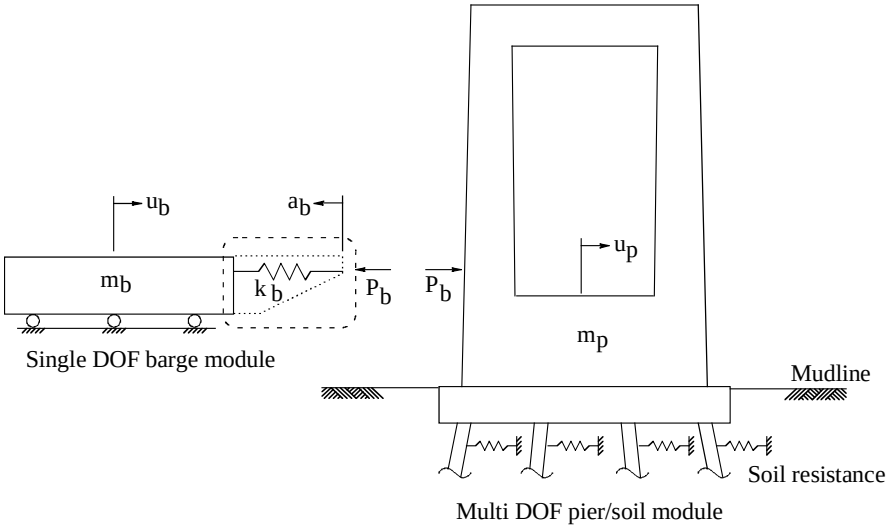

Figure 2.2 Barge and pier/soil modules coupling

Barge and pier responses are analyzed separately in the two distinct numerical modules with FB-Multipier, however, the displacement and the contact force between the barge and pier model are coupled together. Impact forces are actually computed by the barge module using a pre-computed load-deformation relationship for the barge bow. At each time step within the dynamic analysis, the barge module estimates the impact force for the time step based on the current relative displacement between the barge and pier at the impact point. This estimated impact force is then refined using an iterative convergence technique (Consolazio et al. 2005) to satisfy the dynamic equation of motion for the barge. Once the computed impact force has converged, the force is applied to the pier/soil module (FB-Multipier) as an external load. The pier/soil module uses this load to set up the dynamic equilibrium equation for the pier. The estimated pier displacement is iterated until it satisfies dynamic equilibrium, then the displacement of the pier at the impact point is extracted and sent to the barge module for the next time step. The method has been shown to be very efficient in terms of analysis time and effort (Consolazio et al. 2005).

2.4 Contact-Impact Finite Element Analysis

Moving to a level of analysis complexity exceeding that of FB-Multipier, barge impact loads and pier responses can be most accurately assessed through the use of general-purpose dynamic finite element codes (e.g. LS-DYNA, ADINA, ANSYS) that contain robust contact-impact algorithms. In addition to contact, the codes must also include the ability to represent nonlinear material behavior, geometric nonlinearity and dynamic response. Using such codes involves the development of detailed finite element models of the barge, pier and pile-soil-cap interaction. Thus, there is a substantial

investment of resources that must take place prior to achieving useful results. Additionally, such analyses are computationally expensive requiring significant computer resources. Nevertheless, a great deal of insight may be gained by conducting this sort of analysis and if maximum accuracy is desirable, this type of analysis may be required.

In preparing barge and pier models, it is crucial to include accurate geometric, material and inertial properties. Modeling of the barge bow is very important to obtain correct impact forces and properly account for energy dissipated during impact. To achieve this, the barge bow must be modeled using a high-resolution mesh and all elements must be defined as potentially coming into contact with one another. This is very important since it affects the nonlinear crushing behavior of the barge bow. The other very important contact consideration, which determines the accuracy of the impact forces, is specification of a contact interface between the barge bow and the pier column. This contact is responsible for imparting load to the pier as a results of momentum transfer between the barge and pier and allows impact forces to be computed as part of the coupled analysis.

CHAPTER 3
EXPERIMENTAL INVESTIGATIONS OF STRUCTURE AND SOIL RESPONSE TO BARGE IMPACT LOAD

3.1 Introduction

Since the collapse of the Sunshine Skyway Bridge in 1980, the safety of bridges crossing navigable waterways has been a great concern. In 1991, AASHTO adopted the final report of a research project aimed at developing vessel collision design provisions. The project was sponsored by eleven state departments of transportation and the Federal Highway Administration and yielded the Guide Specification and Commentary for the Vessel Collision Design of Highway Bridges (AASHTO 1991). In 1994, AASHTO adopted LRFD bridge design specifications incorporating the 1991 vessel collision provisions as an integral part of the bridge design criteria (Knott 2000). These documents provide a method to determine equivalent static collision loads. Unfortunately, the development of the AASHTO method had to be based on very little experimental data that was obtained from reduced-scale tests.

3.2 Barge Impact Experiments by U.S. Army Corps of Engineers

In 1993, U.S. Army Corps of Engineers (USACE) headquarters issued a Corps-wide analysis procedure for design and evaluation of navigation structures. However, after several years of using the procedure for the design of lock wall projects, it was apparent that the calculated impact force values were too conservative because of the assumption that the barge hull would be crushed in every collision. The single degree of freedom model used in the analysis procedure did not account for energy dissipation

within the mass of the barge flotilla during break-up. Instead, the model assumed that this energy would need to be imparted to the impacted structure or dissipated via crushing of the barge hull. As a result, the impact force, which is related to the crushing energy, is overestimated.

To address this issue, a series of full-scale barge impact experiments were conducted at Gallipolis Lock at Robert C. Byrd Lock and Dam, West Virginia to measure the normal impact force of a barge imparted on the lock wall. The experiments used a fifteen-barge commercial flotilla of jumbo open-hopper barges impacting the lock wall. The experiments ranged in impact angles from 5 to 25 degrees and in impact velocities from approximated 0.5 to 4 ft/sec (0.29 to 2.33 knots). In total, forty-four impact experiments were conducted. The intent of the testing program was to verify and improve the current analytical model used to design inland waterway navigation structures. Using experimental data from these full-scale tests, the USACE developed an empirical correlation between maximum impact force normal to the wall and the linear momentum (immediately prior to impact) normal to the wall. The purpose of the new empirical correlation was to quantify the impact loads in collisions that do not necessarily do damage to either the corner barge of a barge flotilla or to the wall.

3.3 Barge Impact Experiments by UF/FDOT

AASHTO provisions to determine barge impact loads for design of bridge piers against vessel collision were established in 1994. However, very few experiments had ever been conducted to serve the development of the provisions and no full-scale test had ever been performed to quantify barge impact loads on piers. Furthermore, an equivalent static load approach cannot capture dynamic behavior of the structures and soil such as inertial forces and load rate-effects that significantly affect the magnitude and duration of

loading. Preliminary analytical results from research by Consolazio et al. (2002) indicate that AASHTO barge impact provisions appear to over-predict the impact forces in higher energy impact scenarios but under-predict the impact force in lower energy impact. Thus, there was a need for collection of reliable barge impact data including impact load histories, structural displacements and soil response data that can be used to improve the current load prediction procedures.

In 2004, UF/FDOT (Consolazio et al. 2005, Bullock et al. 2005) performed full-scale barge impact tests on the old (now demolished) St. George Island causeway bridge near Apalachicola, Florida. The test involved the use of a deck barge striking bridge piers in series of impact scenarios on impact resistant Pier –1 and a non-impact resistant Pier-3 at varied speeds. Piers 1 and 3 were chosen for testing due to substantial differences in their foundation types, structural resistances, and expected modes of response. Pier-3 was impacted both with and without the superstructure (to investigate superstructure effects) and Pier-1 was impacted without the superstructure. During each collision test, time-varying parameters of structure and soil behavior were measured. Data collected during the tests is compared later in the thesis to corresponding finite element analysis results to calibrate the models so that the physical system behavior observed in the experiments is captured. Within scope of the thesis, the research focuses on investigating Pier-1 responses under the barge impact loading and improving the Pier-1 finite element model. Data from impact test designation P1T7 (Pier 1, Test 7) are selected for discussion, calibration and analysis using finite element models.

Dynamic barge impact load prediction using finite element analysis requires proper modeling of barge, pier and soil. Magnitude and duration of impact loads are affected by

numerous factors such as the mass, velocity, structural configuration of the barge; mass, stiffness and structural configuration of the piers; and properties of soil. By using the experimentally measured impact load histories as prescribed loads in pier analyses, pier models can be calibrated without need for inclusion of a separate the barge model. In-situ soil data calculated from SPT (Standard penetration test), CPT (Cone penetration test) are used to develop nonlinear load-deformation p-y curves that represent the behavior of soil. Experimentally derived dynamic p-y curves are also incorporated in the soil model to capture the increase of resistance due to dynamic behavior of soil. Soil pressure at the front and back of the pile cap and seal are used to refine the soil model to account for the large static and dynamic contribution of the soil resistance on embedded pile caps. By including the measured dynamic parameters of soil, the mechanism of load transfer to the soil and energy dissipation can be properly represented. Pier analysis results using time-varying prescribed loads such as pier displacements, pile shear forces, soil reactions on structures, and pile deflections will be compared to those measured experimentally during impact tests to validate the pier and pile-soil-cap interaction models.

CHAPTER 4
STRUCTURAL MODELING

4.1 Introduction

Pier-1 was the main channel pier of the old St. George Island Causeway Bridge (Figure 4.1) and possessed significant impact resistance provided by soil surrounding the embedded pile cap. To investigate the dynamic resistances and calibrate the soil modeling Pier-1 was chosen for finite element modeling, analysis, and calibration.

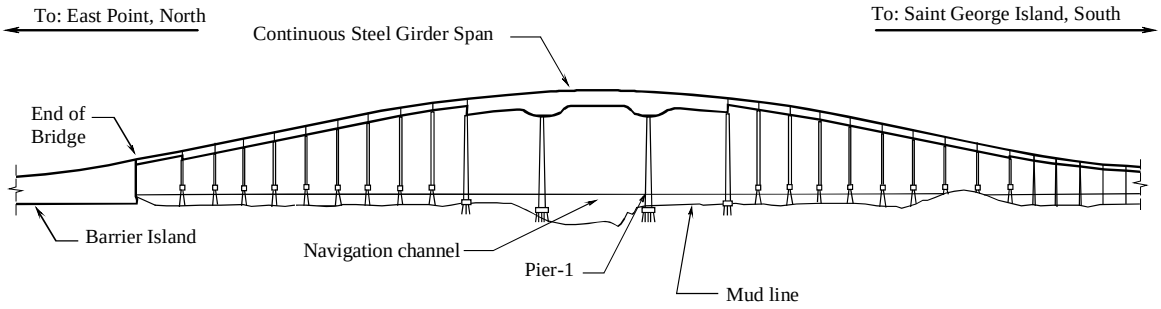

Figure 4.1 St. George Island Causeway Bridge

Two different finite element programs were used in this study: the general-purpose finite element program LS-DYNA (LSTC 2003) and the FB-Multipier (Florida BSI 2005) pier analysis program. LS-DYNA uses an explicit time integration method. It has strong capabilities in dynamic analysis and a variety of nonlinear material models and element types. LS-DYNA also incorporates advanced analysis features relating to large deformation, nonlinear material behavior, and contact detection. In contrast, FB-Multipier is not a general purpose code but rather a finite element program designed specifically for the analysis of bridge piers. FB-Multipier has the ability to account for both geometric and material nonlinearity. Furthermore, many other features such as the

ability to assess the demand-to-capacity ratios of pier elements model soil-pile interaction have made the FB-Multipier program a useful tool for pier design.

4.2 LS-DYNA Model of Pier-1

Pier-1 was the largest pier of the old St. George Island Bridge. It had two massive concrete columns and a large shear wall designed for lateral force resistance near the pile cap. In LS-DYNA, eight-node solid elements were used to model all concrete components of the pier structure including pier columns, bent cap, lateral stiffening shear wall, cap and tremie seal. By using solid elements, the distribution of mass in the piers for dynamic effects can be accurately represented. The pier construction drawings allowed for a construction joint at the interface of the pier superstructure and the pile cap, however, inspection of the construction joint showed that the joint does not affect the stiffness of the pier. Therefore the pier can be modeled as if it was constructed monolithically, that is, the finite element meshes of pier elements (including the pier columns, shear wall and pile cap) share common nodes at their interface (Figure 4.2). LS-DYNA also has an option to join dissimilar meshes as if they were constructed monolithically by using the *CONTACT_TIED_NODES_TO_SURFACE_OFFSET contact option. This option allows different parts of different mesh resolution to be joined together without requiring coincident nodes at interface locations. The option was used to tie the seal and the cap together by tying nodes of the seal top to the bottom surface of the cap (Figure 4.2).

Concrete portions of the pier near the impact region were model with a higher resolution mesh to prevent the elements in this region from undergoing severe distortion, which may produce hourglass deformation modes and erroneous results. To further

prevent the development of hourglass energy, pier components were assigned fully-integrated finite element formulations.

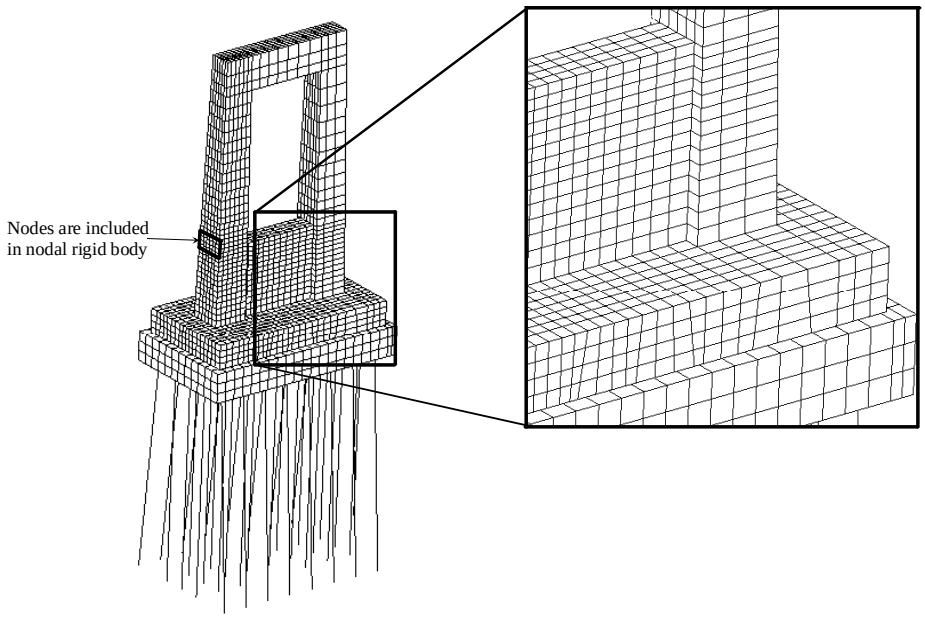

Figure 4.2 LS-DYNA finite element model of Pier-1

For an analysis in which the time-varying load are prescribed, nodes in the pier column at the location where the barge head log makes contact with the pier, are defined with *CONSTRAINED_NODAL_RIGID_BODY so that the prescribed point impact load can be distributed uniformly (Figure 4.2).

Resultant beam elements were used to model the steel H-piles. These elements were extended into the under side of the pile cap to represent the true embedment length of the piles. Each pile consisted of an array of beam elements, each four feet in length and having the cross sectional properties of HP14x73 steel piles.

As part of the full-scale test (Consolazio et al. 2005), an instrumented pile was drilled through the pile cap and driven through the underlying soil to measure the lateral displacements and forces of the pile, and to derive soil response (Bullock et al. 2005). The finite element model of the instrumented pile is included in the Pier-1 model to

compare the pile behavior between computer simulation and impact test. The instrumented pile is modeled using resultant beam elements. All resultant elements in the pile model have lengths of four feet except the element at the pile bottom-tip which has a length of 3.5 ft. Location of the instrumented pile is shown in Figure 4.3. The instrumented pile is modeled as rigidly connected to the seal at the top because the actual field installation of the pile involved drilling through the seal concrete and grouting and bolting the pile to the pile cap. The fixed head assumption is then appropriate for the purpose of comparing the pile lateral displacements, pile shears, and the lateral reaction from soil along the pile depth as predicted by LS-DYNA and as measured experimentally. However, this assumption is not sufficient to permit pile axial load comparisons because the actual instrumented pile was not fully axially clamped to the cap and was observed vertically slip in the grouted hole to some degree during testing. The instrumented pile was constructed from an outer shell of ZW drill casing (8-5/8 in outer-diameter and 8 in inner-diameter, F_y=80 ksi) and a hollow reinforced concrete inner shaft (Bullock et al. 2005). Bending stiffness of the instrumented pile used in the finite element model was derived from moment-curvature data that was obtained from laboratory testing of the instrumented pile.

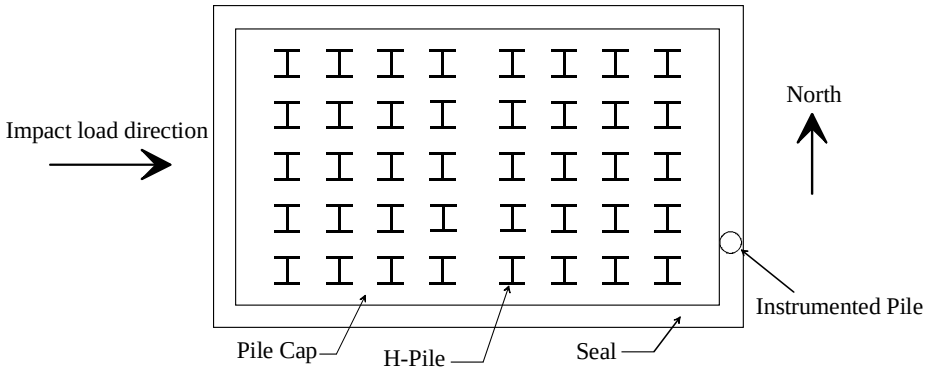

Figure 4.3 H-pile and instrumented pile arrangement

Since the experimental impact loads on Pier-1 were non-destructive in nature, pier concrete cracking and yielding of the H-piles were not expected. Thus, the material model *MAT_LINEAR_ELASTIC was used for both the concrete pier and H-piles. Material values used for the linear elastic material model of the concrete pier components and steel H-piles are presented in Table 4.1.

Table 4.1 Material values used for concrete and steel H-piles

	Concrete parts	**Steel H-piles**
Unit weight	150 pcf	490 pcf
Modulus of elasticity	4415 ksi	29000 ksi
Poisson	0.2	0.3

4.3 FB-Multipier Model of Pier-1

FB-Multipier uses beam elements to model the pier columns and pier cap. The five-foot thick pile cap is modeled using nine-node flat shell elements. The use of beam and flat shell elements greatly reduces the number of degrees of freedom in comparison with the solid elements used in an LS-DYNA model. Therefore, the FB-Multipier simulation usually takes significantly less analysis time than corresponding LS-DYNA simulations.

The steel H-piles and instrumented pile were also modeled using beam elements. Piles are connected to the pile cap through shared nodes at the pile heads. Since the pile cap is modeled with flat shell elements, the effective length of piles extends from the pile bottom-tip to the midplane of the pile cap. This is not desirable because the lateral stiffness of the pier is underestimated. Furthermore, in addition to the five-foot thick pile

cap, Pier-1 also has a tremie seal attached immediately below the cap. The seal is six feet thick and the H-piles are rigidly embedded within the seal. Therefore, the true effective length of the H-piles is from the pile tip to the bottom of the tremie seal. To correctly represent the lateral stiffness of the pier and the fixed-head condition of piles at the seal bottom, cross braces were added between the piles (Figure 4.4). The instrumented pile was also braced to ensure fixity of the pile head. Each cross brace connects a node in an H-pile at the elevation of the tremie seal bottom to a node at the elevation of the pile cap midsurface. The section properties and dimensions of the cross braces were selected to be sufficiently stiff such that the fixity of the pile heads was ensured.

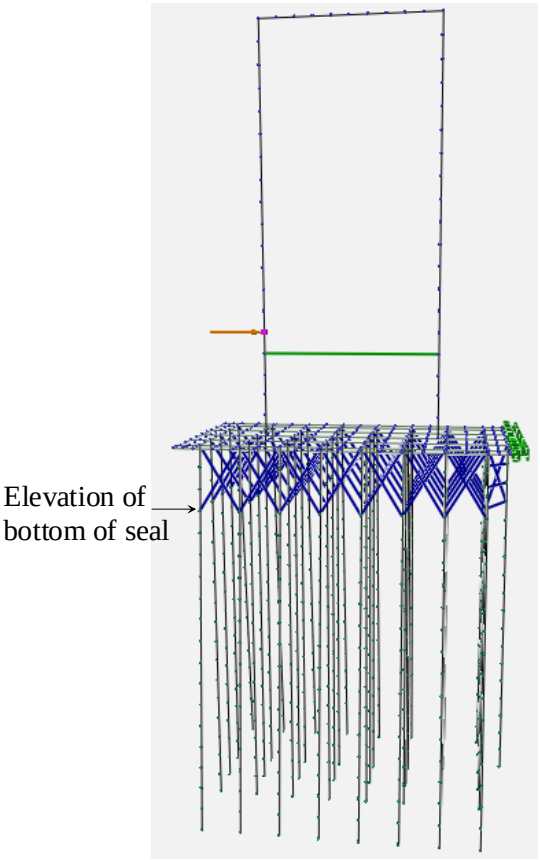

Figure 4.4 FB-Multipier finite element model of Pier-1

CHAPTER 5
DYNAMIC PILE-SOIL-CAP INTERACTION MODELING

5.1 Introduction

Dynamic responses of a bridge pier to barge impact loads are influenced by various factors in which soil-pile and soil-cap interactions play an important role. It is necessary to adequately model the resistance of the surrounding soil to the movement of the bridge pile and cap. Traditional methods of modeling the interaction between the piles and the soil by using nonlinear p-y, t-z and q-z curves that represent the lateral resistance, skin friction, and end bearing resistance correspondingly give good results for static loading or slow cyclic loading. However, a justifiable prediction of pier responses during vessel collision requires a proper evaluation of dynamic soil-pile interaction by taking into consideration various aspects such as radiation damping, degradation of soil stiffness under cyclic loading, nonlinear behavior of soil, pile-soil interface conditions, and lateral cap resistance. For these reasons, dynamic responses of soil and pile from the full-scale testing are used to calibrate the model and investigate the sources of soil resistance that might act on the piles and pile cap during impact events.

5.2 Description of Soil

Modeling the load-deformation behavior of soil requires soil properties to be determined. Therefore an in-situ testing program was carried out (Bullock et al. 2005) using a variety of methods to provide geo-technical data for use in computer simulations. Based on the field-testing, SPT and CPT, the soil profile at Pier-1 was developed (Figure

5.1). Soil properties from in-situ tests were then back-computed as presented in (Table 5.1).

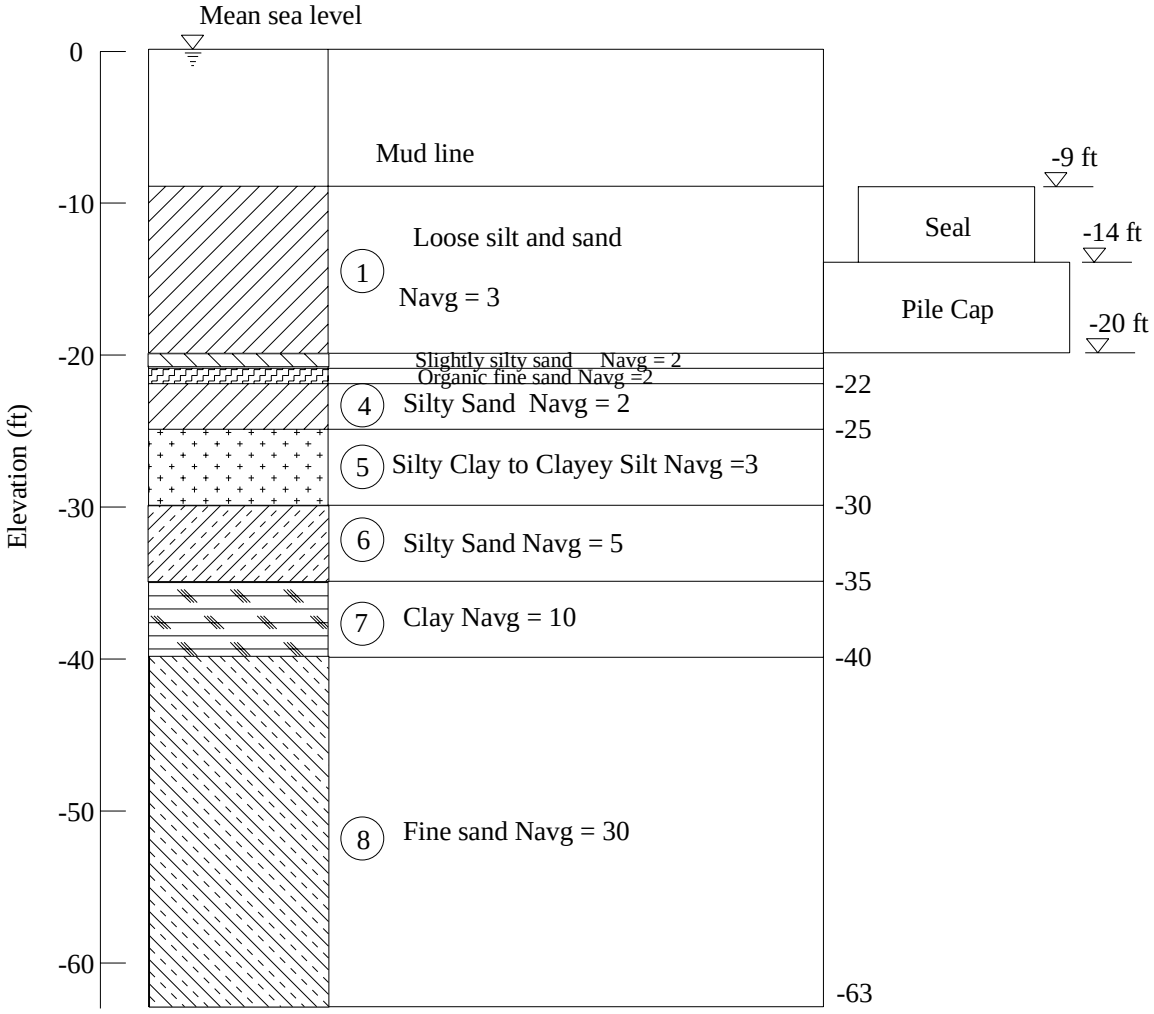

Figure 5.1 Soil profile at Pier-1

Table 5.1 Soil properties from in-situ tests at Pier-1

Layer	Soil Type	SPT	Depth (ft)	Unit Weight (pcf)	Subgrade (kcf)	Undr. Strength (psf)	Strain at 50%	Shear Mod. (ksi)	Poisson's Ratio	Vert. Shear Fail. (psf)
1	Loose Silt and Shell	3	9-20	97.00	43	104	0.02	0.632	0.3	280.1
2	Slightly Silty Sand	2	20-21	106.33	35	NA	NA	1.075	0.3	188.5
3	Organic Fine Sand	2	21-22	104.33	NA	574	0.02	0.145	0.37	161.9
4	Silty Sand	2	22-25	109.67	51	NA	NA	2.043	0.3	188.5
5	Silty Clay to Clayey Silt	3	25-30	97.00	NA	331.33	0.02	0.096	0.2	280.1
6	Silty Sand	5	30-35	109.00	77	NA	NA	4.730	0.3	458.2
7	Clay	10	35-40	99.50	NA	370.67	0.07	0.095	0.35	543.2
8	Fine Sand	30	40-63	125.33	224	NA	NA	23.277	0.37	423.4

5.3 Dynamic p-y Curve

The static p-y curve approach to modeling soil behavior is widely used in static analysis of soil-pile interaction. However using static p-y curves for dynamic analysis without inclusion of the effect of velocity-dependent damping forces may lead to erroneous results. Dynamic soil resistance is higher than static soil resistance due to the contribution of damping and rate effects. El Naggar and Kevin (2000) proposed a method for obtaining dynamic p-y curves. These dynamic p-y curves are generally considered to be a good representation for soft to stiff clays and loose to dense sands. The equation for dynamic p-y curve determination was developed from a regression analysis relating static p-y data, loading frequency, and soil particle velocity. However, analysis results obtained using this dynamic p-y approach are highly dependent on the correct determination of soil properties. In order to better characterize pier response, the dynamic p-y curves measured from the field-testing are directly introduced into the soil-pile model of Pier-1.

From bending strains measured by strain gauges attached along the instrumented pile, the curvature and the moment of the pile through time were determined. Pile displacements (y-values) were calculated through double integration of the curvature equations and the soil reactions (p-values) were derived through double differentiation of the moment equations along the pile through time.

Time histories of pile displacement and soil reactions at elevations from -21ft to -50ft were computed from data measured during impact testing of P1T7. However, the soil around pile cap and the pile head zone carried most of the lateral force. The dynamic component of soil reaction was found to decrease significantly between elevation –21ft

and elevation -26ft. At elevation -21ft, total soil resistance was observed to be well in excess of the static resistance. This increase was attributed to dynamic load-rate effects. However, at elevation -26ft and deeper, extra dynamic resistance was not evident leaving only the static component of soil resistance. For this reason, the dynamic soil reactions and pile displacements at elevation -21ft and -26ft will be the focus of discussion here. Time histories of experimentally determined pile displacements and soil reactions at elevation -21ft and -26ft are shown in Figure 5.2 and Figure 5.3 .

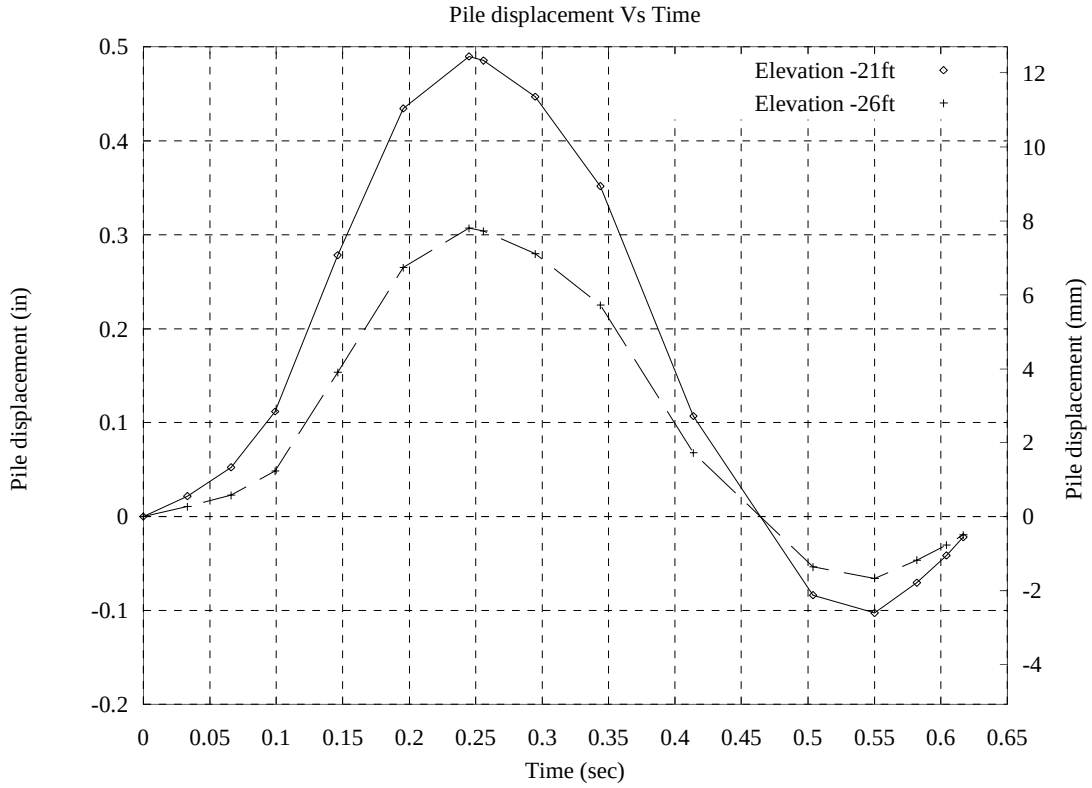

Figure 5.2 Pile displacements vs. time at elevation –21ft and –26ft

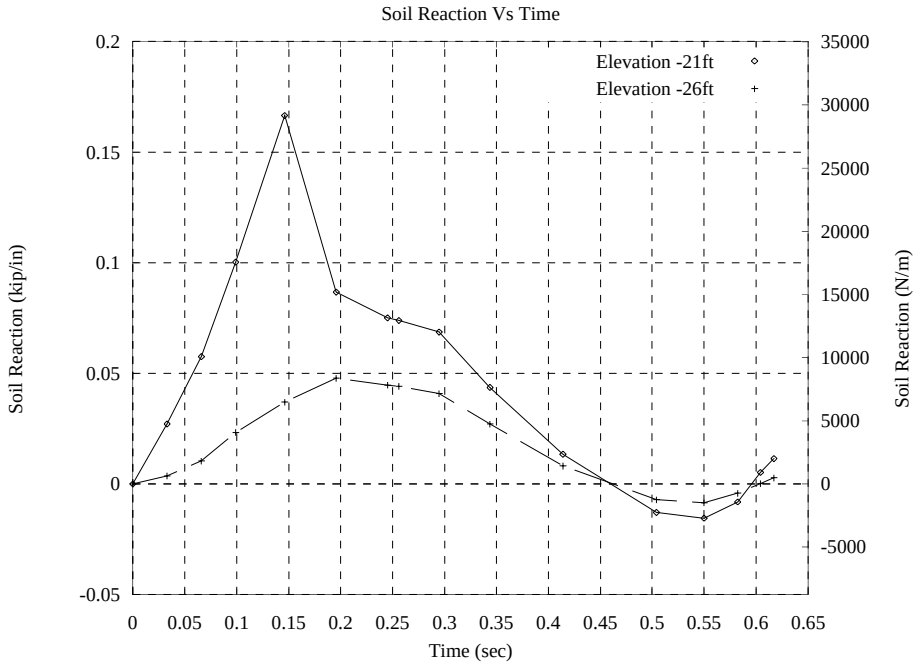

Figure 5.3 Soil reactions vs. time at elevation –21ft and –26ft

It is noteworthy that maximum displacement of the pile head (elevation –20ft) occurs at 0.25 sec but that the maximum soil reactions occur earlier. Soil reactions on the instrumented pile at elevations -21ft and -26ft reach maximum values at 0.15sec and 0.2sec respectively. For static loading, the soil reaction is expected always to be smaller than or equal to the soil reaction corresponding to maximum pile displacement. That is, the soil reaction reaches a maximum value when the maximum pile displacement occurs. However, this need not be the case for dynamic loadings. Under dynamic loading, the soil reaction consists of both a static resistance force and damping (rate-dependent) force. Damping force on a pile is a function of several parameters including rate of loading, particle velocity, and soil properties. In Figure 5.2 , the pile displacement plot has the highest slope at 0.12sec. Consequently, the pile velocity has reached its maximum and the maximum damping force is therefore mobilized. As shown in Figure 5.3 , the maximum soil reactions occur between 0.12sec and 0.25sec. When the pile reaches the

point of maximum displacement and starts to rebound, the pile velocity is reduced to zero and the damping force disappears. At this time, the soil reaction is merely static resistance.

By plotting soil reaction versus pile deflection, the dynamic p-y curves at elevations -21ft and -26ft are presented in Figure 5.4 . To evaluate the dynamic contribution of the damping force to the total soil reaction, static p-y curves at elevation -21ft and -26ft are estimated based on the dynamic p-y curves (Figure 5.5 , Figure 5.6). The static and dynamic p-y curves have the same initial slope and intersect one another at the point of maximum displacement. Figure 5.5 shows that the damping resistance portion may be as large as the static resistance portion. From the pile top down to elevation -26ft, the contribution from damping resistance decreases due to reduction of pile velocity.

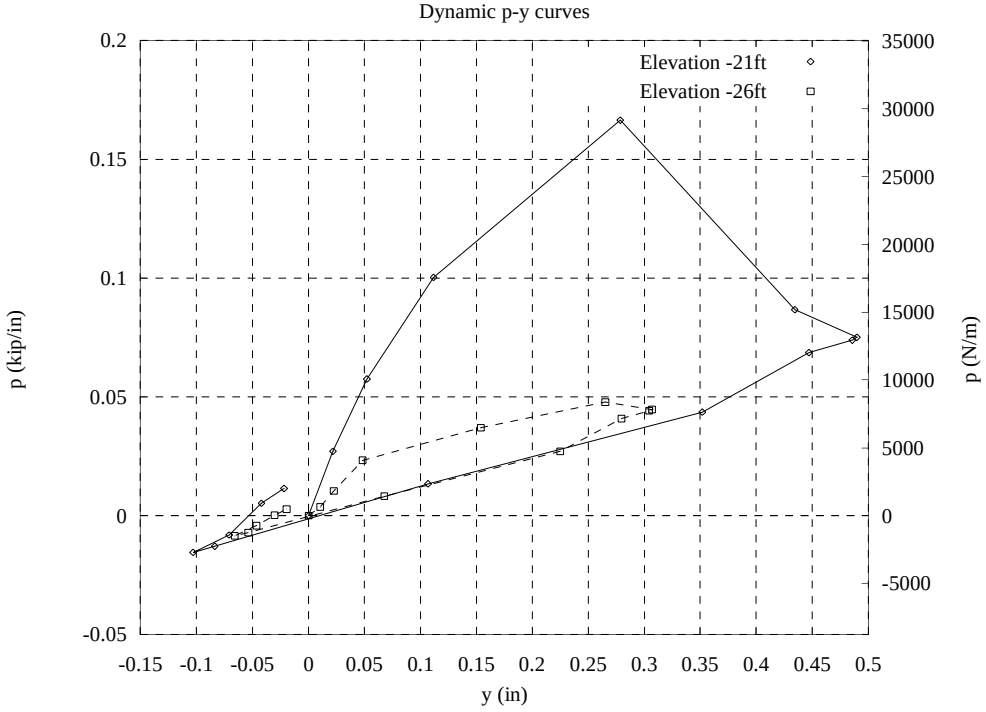

Figure 5.4 Measured dynamic p-y curves at elevation –21ft and –26ft

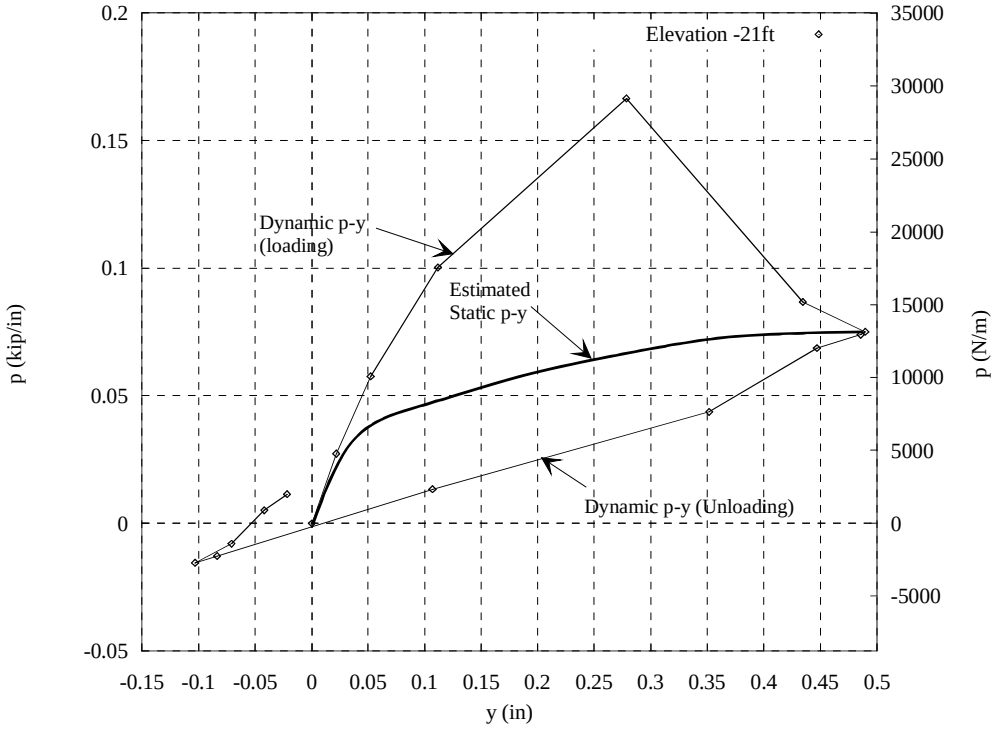

Figure 5.5 Dynamic and static p-y curves at elevation –21ft

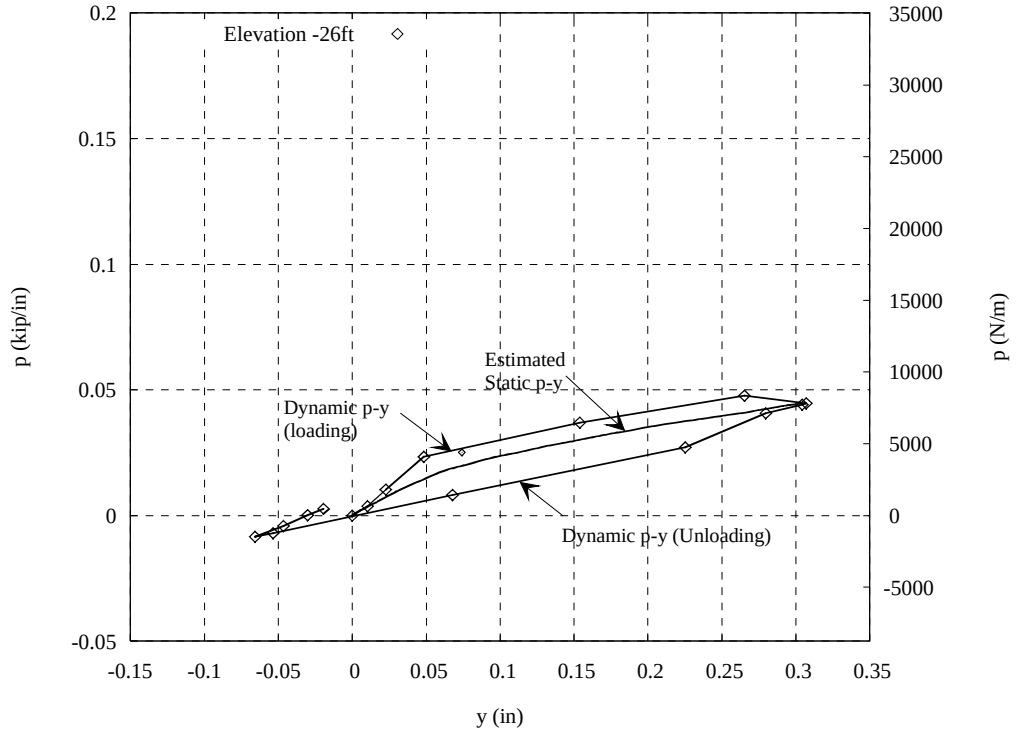

Figure 5.6 Dynamic and static p-y curves at elevation –26ft

In order to model overall pier behavior, it is important to properly represent the contribution of the rate-dependent damping resistance as well as the energy dissipation that is associated with damping. This information must then be combined with the static soil resistance data. Therefore, in this study the experimentally measured dynamic p-y curves were introduced into the soil-pile interaction model. Dynamic p-y curves (Figure 5.5 and Figure 5.6) show that the slope of the unloading curves is smaller than the initial slope of the loading curve and the unloading curves pass through the point of zero displacement with zero force. This indicates that upon unloading and reloading in the negative direction, the piles and the soil are still in contact to some degree. Separation at the soil-pile interface (gapping) often occurs in clays during cyclic loading due to inelastic deformation. But the soil-pile interface for sands may exhibit different behavior. Sands can cave-in resulting in backfilling of sand particles around the pile during cyclic loading. The soil profile for Pier-1 (Figure 5.1) shows that from the pile top (-20ft) down to elevation -26ft, sandy soil behavior is expected.

The pier response observed during impact testing showed that most of the lateral resistance was provided by soil residing above the elevation -32ft. Therefore, the load-deformation relationship of the lateral springs down to this elevation were described using measured dynamic p-y curves. Below this elevation, static p-y curves were used since particle velocities were not sufficient to mobilize dynamic components of resistance.

5.4 Lateral Resistance of the Pile Cap and Seal

Typical procedures for calculating the lateral resistance of a pier usually ignore the contribution of soil surrounding the pile cap (if the cap is embedded). This is simply due to the fact that methods for quantifying such resistance have not been well

established. However, researchers have found that the lateral resistance provided by embedded caps can be very significant. Neglecting soil-cap resistance may lead to inaccuracies of one hundred percent or more (Mokwa 1999). From the design standpoint, neglecting cap resistance means underestimating the foundation stiffness and potentially overestimating the shear, bending moment, and deflection of the piles. As a result, an uneconomical design may follow from such omission. For the purpose of understanding the measured responses of Pier-1, soil-cap interactions must be taken into account.

The pile cap of Pier-1 measures 21ft by 39ft-2in by 5ft thick. The tremie seal below the cap measures 24ft by 42ft-2in by 6ft thick. At the time of the Pier-1 impact tests, the elevation of the mudline corresponded to the top of the pile cap. Thus both the pile cap and the seal were surrounded by soil and therefore the soil resistances on cap and seal have been included in the finite element model of Pier-1. Without including the lateral resistances of soil at the pile cap and seal, computer simulations using LS-DYNA and FB-MultiPier predicted excessive pier displacements in comparison to those obtained from experimental impact testing. Clearly, this emphasizes the considerable resistances provided by the cap and the seal.

Mokwa (1999) developed procedures for computing cap resistance and used hyperbolic p-y curves to represent the variation of the resistance with cap deflection. Hyperbolic p-y curves are the functional form of the ultimate passive force and the initial elastic stiffness of the embedded pile cap.

Because soil-cap interaction during an impact event is of a dynamic nature, Mokwa’s approach may not be applicable. The current state of knowledge and practice regarding lateral cap resistance, especially dynamic soil-cap interaction and the

mechanics of load transfer, is still limited. To gain a better understanding of soil-cap interaction and quantify the lateral cap resistance, push-in stress cells were installed (during the experimental program) in the soil mass at both the lead and trailing sides of the cap and tremie seal (Bullock et al. 2005). Soil forces on the cap and seal during impact testing were determined from the resultant of changes in stress of the front and rear sides of the pier.

Figure 5.7 shows the passive force on the cap and seal experimentally measured during impact testing P1T7. Maximum passive forces on the cap and seal are 60 kips and 140 kips respectively in comparison to the measured peak impact load of 864 kips. The total of 200 kips shows considerable contribution to the lateral resistance of passive pressure developed on the cap and seal. To understand the dynamic soil-cap interaction, the experimental data are normalized and plotted in Figure 5.8 . Displacement at elevation -20ft (seal bottom) and displacement at the top of the pier shear wall (+6ft) agree well, therefore the displacement and velocity behavior of both the cap and seal may be adequately represented by that of the top of the shear wall.

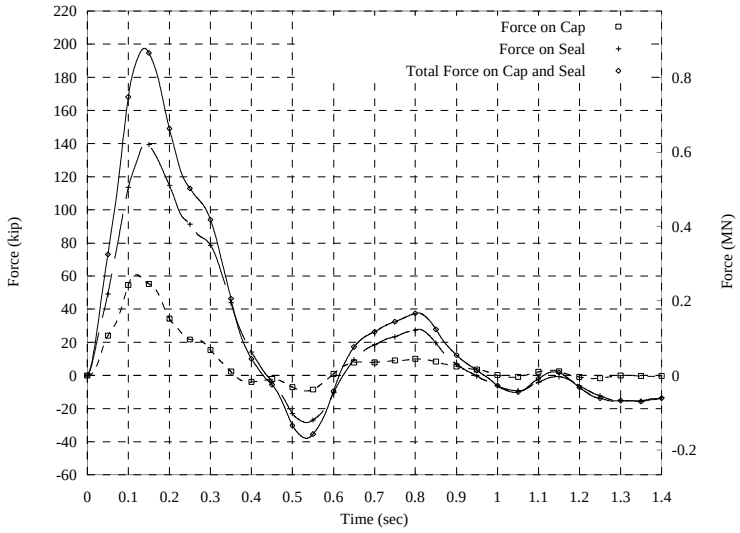

Figure 5.7 Measured resultant passive force on cap and seal during impact P1T7

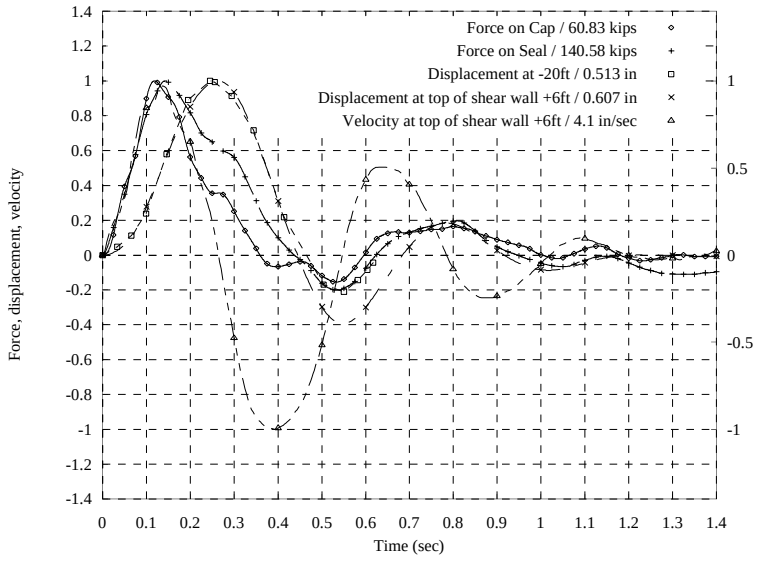

Figure 5.8 Normalized experimental data plot during impact P1T7

As shown in Figure 5.8 forces on the cap and seal show similarities to the behavior of the soil reaction on the instrumented pile discussed in Section 5.3 . If the maximum force occurs at a time close to the time of maximum velocity, the damping force dominates over the static force and the response is highly dynamic. If the maximum force occurs at the time of maximum displacement, the resistance is purely static. P1T7 is a highly dynamic test scenario in which the barge velocity is 3.41knots (5.76 ft/sec) and the kinetic impact energy is 622 kip-ft. Therefore, peak force on the cap and seal occurring at about the time that maximum velocity is expected.

The dynamic load-displacement curve for the cap and seal and the estimated static loading curve are presented in Figure 5.9 . Contribution of damping forces at the lead side during the first cycle is very significant (~120 kips). When the cap and seal reach the maximum displacement, the damping force reduces to zero and the static passive force developed on the cap and seal is approximately 100 kips. The area between the dynamic loading curve and the estimated static curve represents the energy dissipation due to

radiation damping, whereas the area between the estimated static loading curve and the unloading curve represents the energy dissipation caused by hysteretic damping.

Forces acting on the lead and trail sides of the cap and seal are shown separately in Figure 5.10 . These forces actually correspond to the change in force on the cap and seal during impact because at rest, the cap and seal already have the equal in-situ force at both sides. Positive values mean an increase of soil force on the cap and seal and vice versa. At approximately 0.44sec, the displacement of the cap and seal is zero (the pier has rebounded to its original position), however, the soil force on the trail side is still positive. This indicates that the soil on the trail side caved-in when the cap and seal moved in the direction from the trail side to the lead side. Soil backfilling provides contact between the cap/seal and the surrounding soil allowing continuous resistance when the pier moves in the reverse direction. When passing through zero displacement, the non-zero velocity of the pier results in damping force thus providing additional resistance. Soil stiffness may not contribute to the increase of resistance because the static soil force on the cap/seal at this position may not be larger than that in the at rest condition (due to soil remolding).

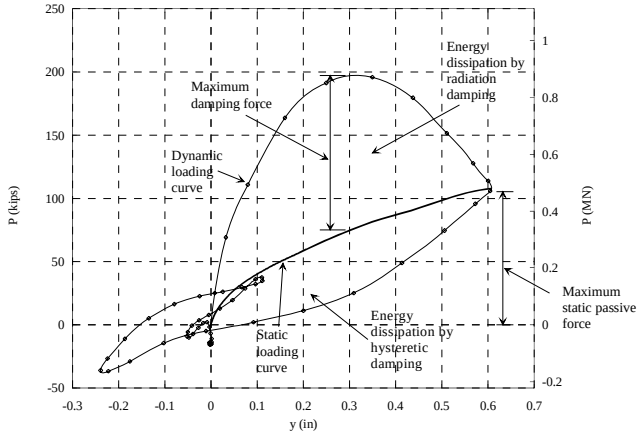

Figure 5.9 Experimentally measured load-displacement curve of the cap/seal during impact P1T7

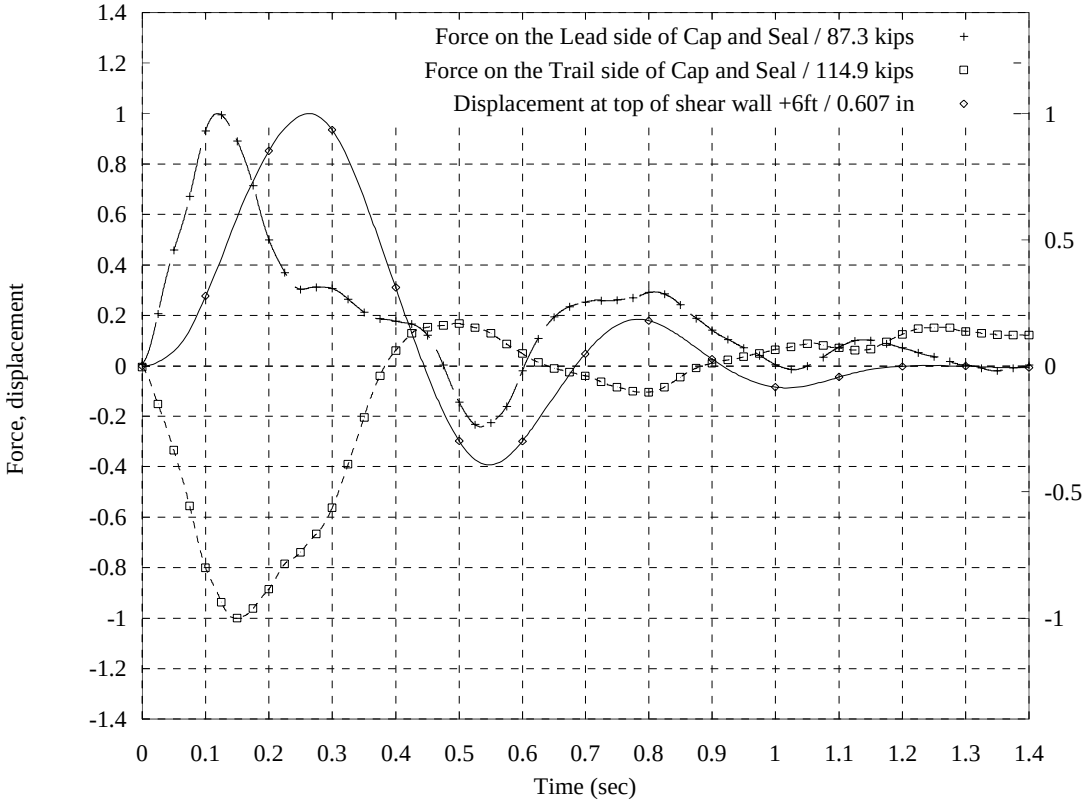

Figure 5.10 Experimentally measured normalized forces and displacement during impact P1T7

When the displacement of the pier goes through the original (zero) position at approximately 0.68 sec, the soil force on the lead side is positive due to the backfilling of the soil at the lead side. This behavior is reasonable because the soil surrounding the cap and seal is sandy in nature (Figure 5.1).

5.5 Soil-pile Interaction Model of Pier-1 in LS-DYNA

In this study, soil-pile interaction is modeled for LS-DYNA analysis using nonlinear springs positioned at nodes along the length of the piles. At each pile node (at 4 ft vertical intervals), lateral resistance is modeled by using two perpendicular sets of

soil springs and pile skin resistance is modeled using one vertical axial spring. An axial spring at the pile tip is used to model end bearing resistance. Lateral spring curves are computed using the static p-y curve construction approach and dynamic p-y curves are derived from experimentally measured data. An illustration of the spring arrangement at each pile node is shown in Figure 5.11 .

A typical H-pile of Pier-1 with the soil-pile interaction springs added is shown in Figure 5.12 . Figure 5.12 also shows the addition of 1-node point elements at the anchorage points of each soil spring. LS-DYNA has a requirement that all discrete spring elements be attached to nodes of finite mass. The anchorage point nodes of the soil springs are only attached to the spring elements which have no mass. Therefore, single-node point mass elements were added to satisfy the software requirements. The point masses are not fixed; instead, they are constrained to move with the pile nodes to prevent incorrect spring alignment (discussed in detail later). For this reason, the masses of these point elements are chosen to be very small so that gravity effects are negligible.

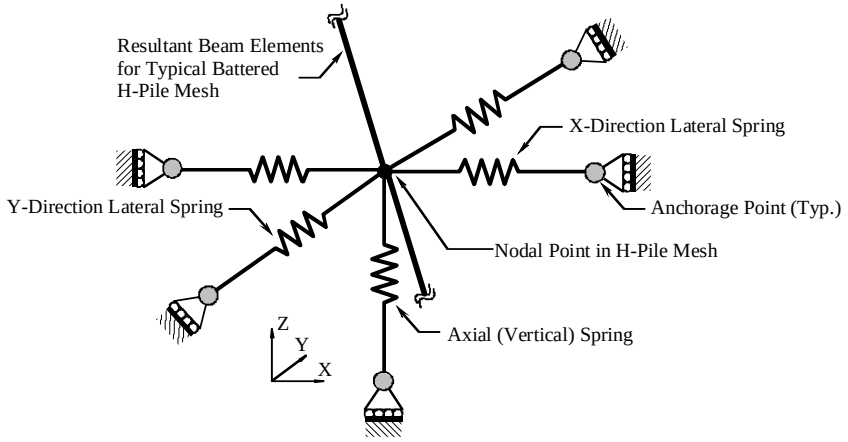

Figure 5.11 Soil spring grouping at a typical node in the Pier-1 model

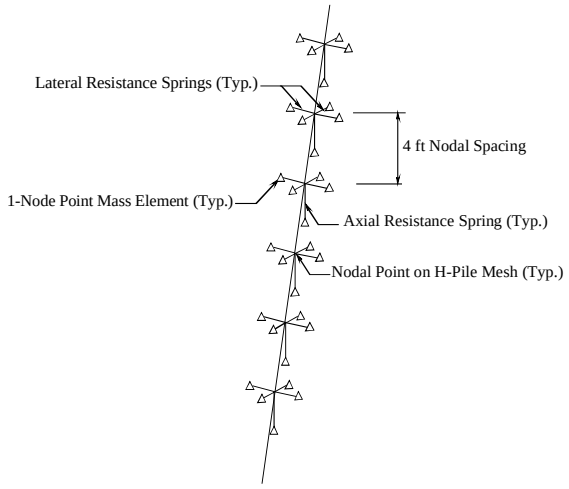

Figure 5.12 Typical H-pile with soil resistance springs in Pier-1 model

5.5.1 Lateral Soil Resistance

The lateral resistance springs were modeled using the LS-DYNA non-linear spring material model `*MAT_SPRING_GENERAL_NONLINEAR` which allows specification of separate loading and unloading curves describing the force versus displacement relationship for the spring. Both curves may be linear or nonlinear. The non-linear curves may represent the lateral behavior of soil-pile interaction in the static or dynamic manner. Numerical methods for the determination of the static or low frequency cyclic soil-pile interaction equations have been derived empirically through extensive experimental testing and analytical modeling. Factors that have the most influence on the p-y curves are the soil properties, pile geometry, nature of loading and the soil depth where the lateral resistance capacity is desired. Due to the dependence on the depth, and variability of soil conditions along the length of the piles, p-y curves at each vertical elevation are theoretically unique. The combination of using two zero-tension springs on both sides of piles in each lateral direction allows energy dissipation through hysteretic damping and gap formation of the soil to be represented. The behavior of the gap formulation is presented in Figure 5.13 .

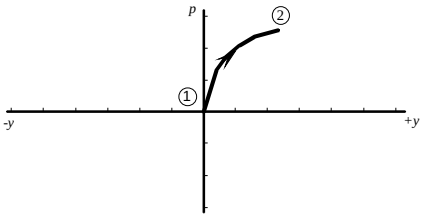

a) Loading of positive deformation

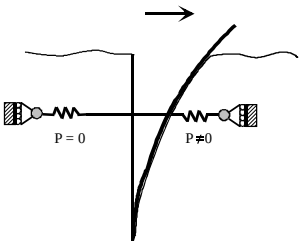

b) Depiction of state 1 to 2

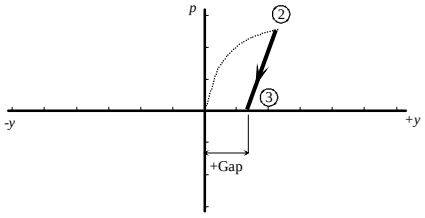

c) Unloading of positive deformation

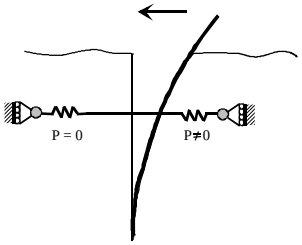

d) Depiction of state 2 to 3

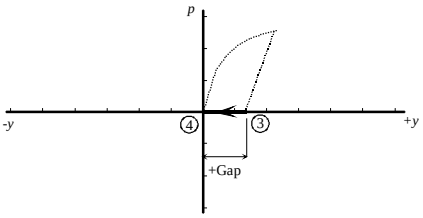

e) Moving within the gap

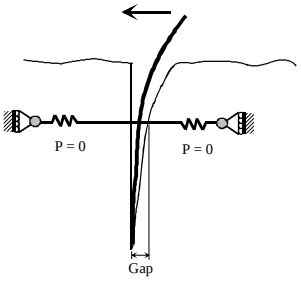

f) Depiction of state 3 to 4

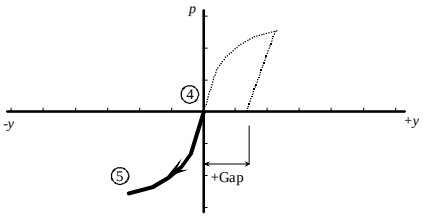

g) Loading of negative deformation

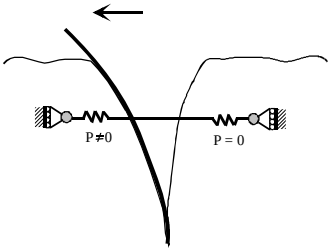

h) Depiction of state 4 to 5

Figure 5.13 Force vs Deflection (p-y curve) gap model formulation

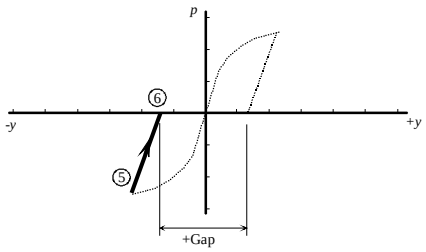

i) Unloading of negative deformation

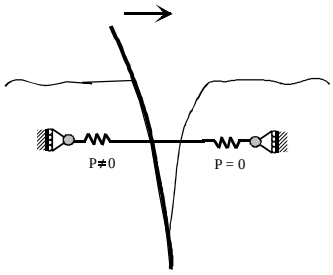

j) Depiction of state 5 to 6

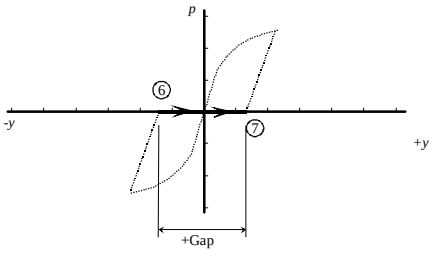

k) Moving within the gap

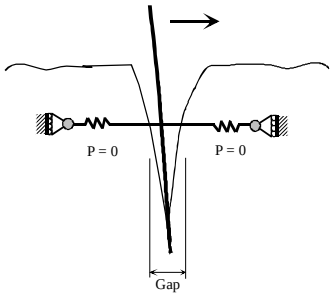

l) Depiction of state 6 to 7

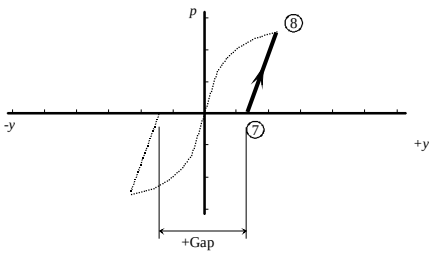

m) Loading of secondary positive deformation

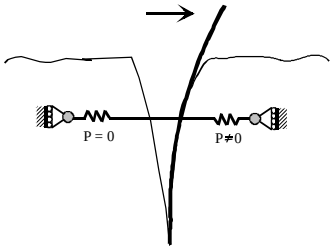

n) Depiction of state 7 to 8

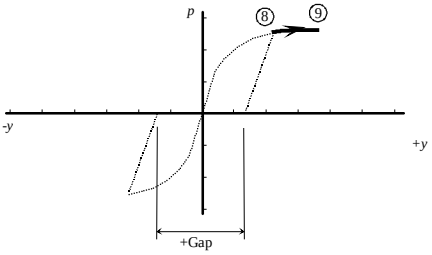

o) Loading of secondary positive deformation

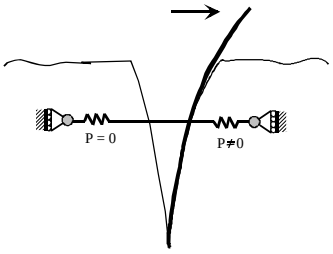

p) Depiction of state 8 to 9

Figure 5.13 Force vs Deflection (p-y curve) gap model formulation

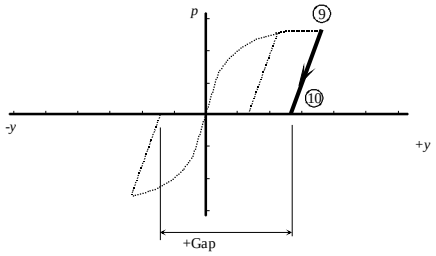

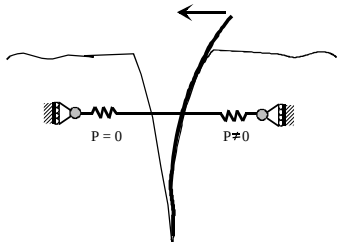

q) Unloading of secondary positive deformation r) Depiction of state 9 to 10

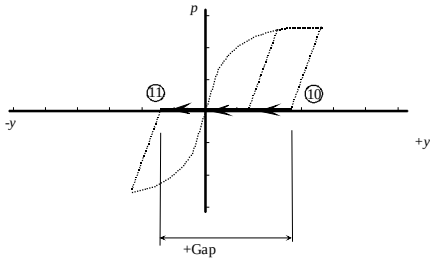

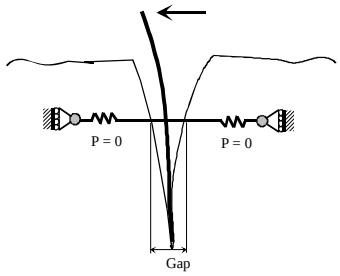

s) Moving within the gap t) Depiction of state 10 to 11

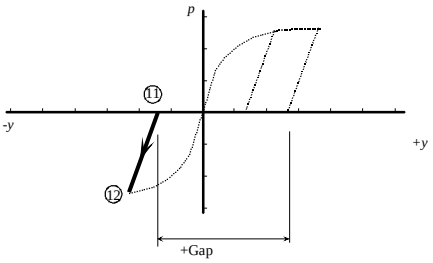

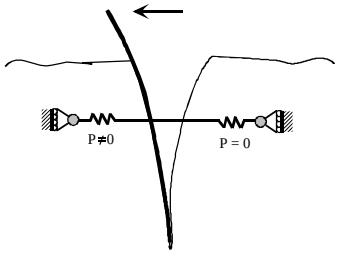

u) Loading of secondary negative deformation v) Depiction of state 11to 12

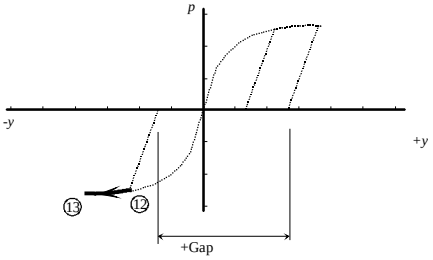

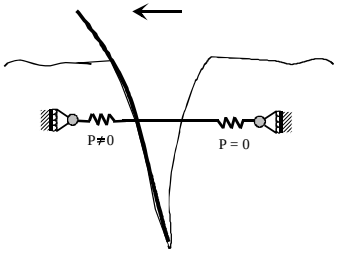

x) Loading of secondary negative deformation y) Depiction of state 12 to 13

Figure 5.13 Force vs Deflection (p-y curve) gap model formulation

From state 1 to 2, the pile moves in the +y direction and pushes on the undisturbed soil. The right spring is compressed with increasing force following the p-y loading curve. The left spring provides no resistance force. As the pile reaches a maximum displacement, it starts to rebound. The compressed soil unloads following the unloading curve (state 2 to 3), which is typically an elastic curve and elastic deformation is fully recovered at state 3. However, due to the nonlinear behavior of the soil, at this state the soil has undergone permanent deformation and a gap is formed. Therefore, from state 3 to 4, the soil stops following the pile and the pile is free to move without resistance (the force in both springs is zero) until it reaches the soil in the -y direction.

From state 4 to 5, the pile pushes on the soil in the -y direction. The soil loads following the p-y loading curve with the assumption that the soil on the -y side of the pile has not been affected by the previous loading in the +y direction. When moving in the reverse direction, the soil unloads and follows the pile during state 5 to 6. At state 6, soil reactions on both sides of pile are zero and a gap in the -y direction has been formed.

Depending on the magnitude of loading and sustained energy in the system, the pile may continue to move through the entire gap (state 6 to 7) and once again reaches the soil in the +y direction (state 7). At this state, the soil loads along the same curve (state 7 to 8) that it previously unloaded along (state 2 to 3). When the load reaches the level equal to that of state 2, the soil will load along the p-y loading curve (state 8 to 9). The next time the load reverse, the soil will unload following the unloading curve (state 9 to 10). At state 10, the gap in the +y direction has been increased. Reversed loading in the -y direction will cause the pile to traverse the entire gap without resistance (state 10 to 11). At state 11, the soil will load along the previously unloaded curve in the -y direction

(state 11 to 12). Once the pile reaches the force level previously reached before unloading in the -y direction, the soil will continue to load following the p-y loading curve. The process continues in the same manner until kinetic energy of the system is fully dissipated.

To distinguish p-y curves of this type from dynamic p-y curves, which includes the effect of damping and load-rate, static p-y curves will from this point forward be referred to as “traditional” p-y curves for static or cyclic loading case. For this study, static p-y curves are incorporated into nonlinear lateral springs from elevation -32 ft down to the pile tip. This is due to the fact that the lateral pile displacements and velocities are an order of magnitude smaller than those at the pile-head. Therefore, damping force and loading rate effect are negligible.

In-situ soil data were used to generate static p-y curves for the nonlinear force-deformation loading curves of lateral springs from elevation -32 ft downward. Static p-y curves were constructed using the Reese, Cox and Koop’s method for sandy soil, and Matlock’s method for soft-clay-in-the-presence-of-water for clayey soils. The Reese, Cox and Koop’s method requires pile diameter, soil depth at the analysis point, and in-situ data such as internal friction angle (ϕ), soil unit weight (γ), and subgrade modulus (k). Because the soil is below water, the submerged unit weight was used. For Matlock’s method, in addition to pile diameter and soil depth at the analysis point, it is necessary to carefully estimate the variation of undrained shear strength (c), submerged soil unit weight with depth, and the value of ε_{50} – the strain corresponding to one-half the maximum principal stress difference. Both methods assume the presence of only a single layer of soil. Before using these methods to construct the static p-y curves, the soil layers

are transformed using the method of Georgiadis (Florida BSI 2005), which is based on the relative capacities of the layers, to obtain an equivalent soil profile with only a single layer. The static p-y curves were defined with displacements up to 12 inches, which is well beyond the maximum deformation of any spring during the Pier-1 impact simulation. Because the p-y curve represents the soil resistance at a particular depth and is defined in terms of soil resistance per unit length versus deflection, load-deflection curves for each spring were obtained by multiplying the "p" values of the p-y curves by the distance between pile nodes (typically 4 ft) that lateral springs attach to. Unloading curves for the lateral springs were defined as elastic curves that had the same slope as the initial slope of the p-y loading curve.

Dynamic p-y curves, used to describe the load-deformation of the lateral springs in the pile head zone, must be carefully processed before introduction into the LS-DYNA soil model. The maximum pile displacement from an LS-DYNA simulation may exceed the maximum pile displacement from the experimentally measured dynamic p-y curves. If no modification is made to the dynamic p-y curves, LS-DYNA will assume that the force of the non-linear spring element is zero whenever the pile displacement exceeds the maximum displacement described in the loading curve assigned to that spring. To prevent this, the experimentally measured p-y curves were extended to accommodate a displacement of up to 1 inch. For the loading curves, the force in the springs will be constant when the pile displacement exceeds the maximum pile displacement of the measured dynamic p-y curves (see Figure 5.14).

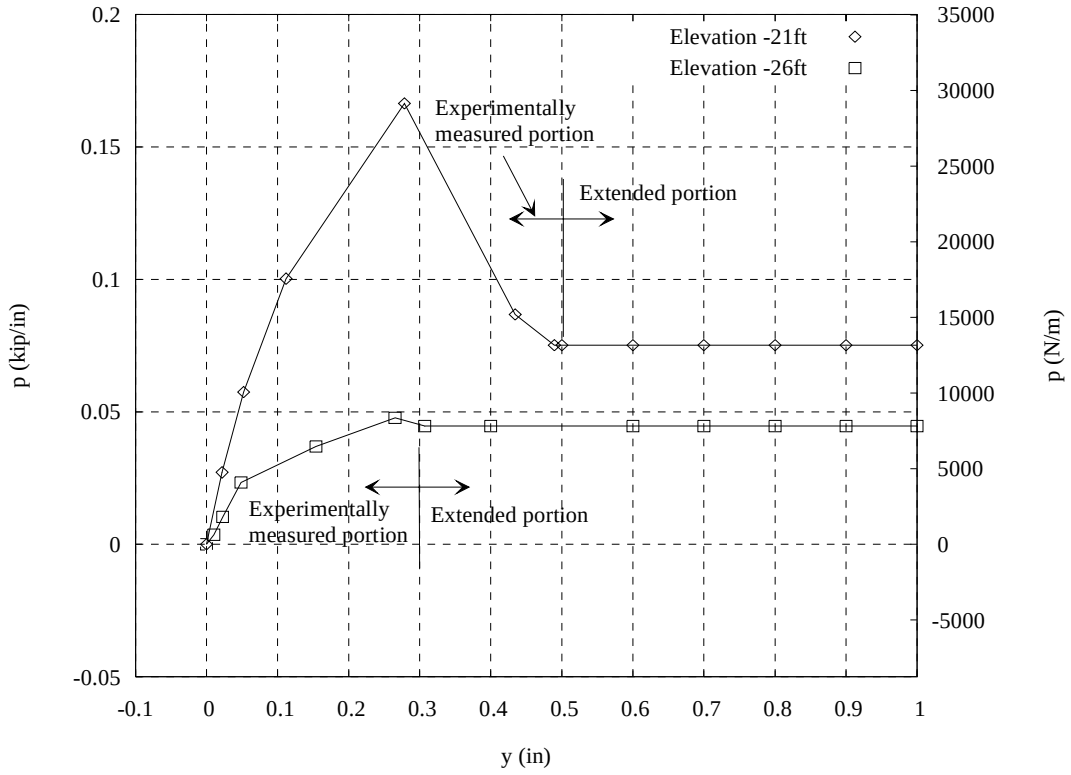

Figure 5.14 Dynamic p-y loading curves for LS-DYNA implementation

5.5.2 Pile Group Effect

Considerable research has been conducted in the area of pile group effects. These studies have shown that average load for a pile in a group will be less than that for a single isolated pile at the same deflection. Piles in trailing rows will carry less load than piles in leading rows. One method to account for group reduction is to scale down the soil resistances (p) from p-y curves generated for single isolated piles. The reduction factor is called a row-multiplier or p-multiplier. The p-multipliers are dependent on both the location of the pile within the pile group, and the pile spacing. During barge impact, the pile group may undergo cyclic motion back and forth turning leading-row piles into the trailing-row piles and vice versa during cyclic reversal. Therefore, the relative position of piles in the group changes with the direction of movement of the pile group. To correctly

represent the soil resistance for dynamic impact simulation, p-multipliers are specified such that they may change depending on the loading direction of the group. The p-multiplier values used in LS-DYNA for lateral soil springs are presented in Figure 5.15

.

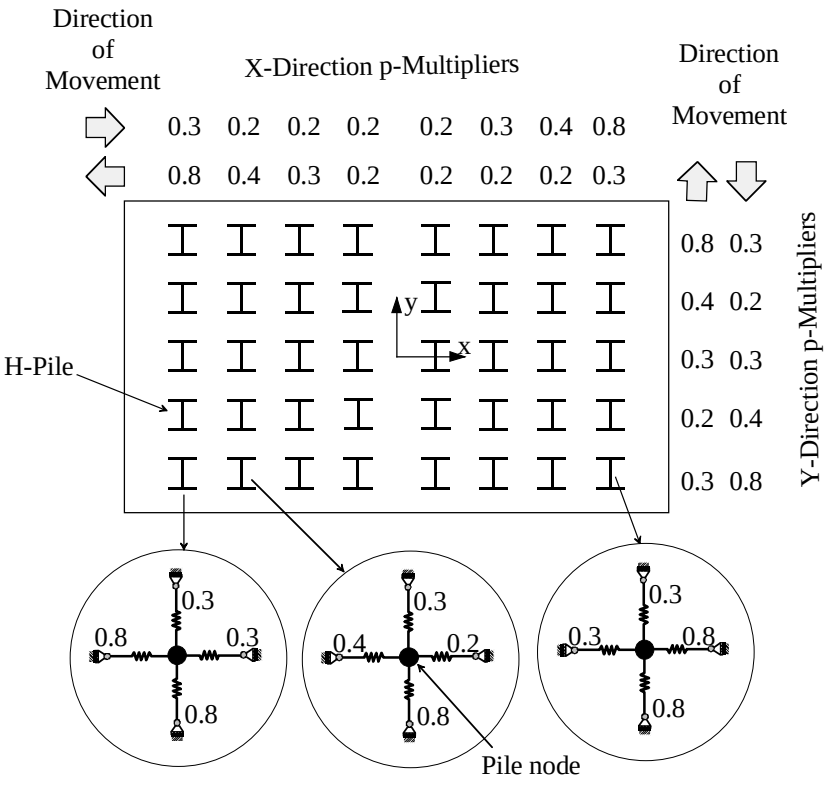

Figure 5.15 P-multiplier for Pier –1 pile group

5.5.3 Axial Skin Friction Along Piles

Barge impact load is transferred from the pier structure to the soil not only through lateral resistance of the soil but also through vertical skin friction of the soil along the pile length. Therefore, in addition to the springs representing lateral soil resistance on the piles, axial springs were also introduced into the model to represent the axial skin friction. At each pile node, an axial spring using the LS-DYNA material model `*MAT_SPRING_NONLINEAR_ELASTIC` was added. This material model is loaded and unloaded along a nonlinear but elastic curve. Load-deformation curves of this type are

known as t-z curves. The t-z curves used for this study were constructed based on a method developed by McVay et al. (1989) using in-situ soil data. In this method, vertical deflection of a node on a pile is calculated as a function of the shear stress at that depth on the surface of the pile. The vertical deflection is also a function of the radial distance outward to a point in the soil where the shear stress is negligible (r_m) - referred to as the radius of the zone of influence. The zone of influence is in turn dependent upon the ratio of the soil shear modulus at the mid-depth of the pile to the soil shear modulus at the bottom tip of the pile. Furthermore, these shear moduli vary with the shear stress in the soil. Thus, the t-z curves vary with the vertical deflection of the pile.

5.5.4 Maintaining Proper Alignment of Soil Springs

Nonlinear springs modeling the soil-pile interaction will not work properly without consideration of spring alignment during the impact simulation. If all three of the translational degrees of freedom of the soil spring anchorage points were fixed, movement of the pile nodes could lead to excessive misalignment of the springs (Figure 5.16). As a result, the lateral soil springs could then erroneously contribute to the axial soil behavior. Similarly, the axial spring could contribute to the lateral behavior of the soil. Even more important, however, is the fact that skewed changes of soil spring alignment will result in a change of the effective lateral stiffness that is imparted to the pile by the soil. In such cases, the lateral displacements of the pile will be erroneously computed.

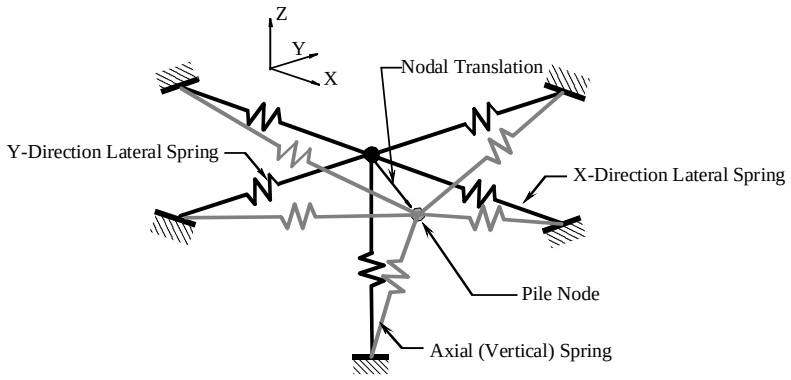

Figure 5.16 Misalignment problem

To ensure that the axial and lateral soil springs remain orthogonal during impact, nodal constraints were employed. Three constraint node sets were defined corresponding to the global x, y and z directions. In the x-direction, nodes 1, 4, 5 and 6 are constrained to move with each other (Figure 5.17 a). In the y-direction, nodes 1, 2, 3 and 6 are constrained to move with each other (Figure 5.17 b). In the z-direction, nodes 1, 2, 3, 4, 5 are constrained to move with each other (Figure 5.17 c).

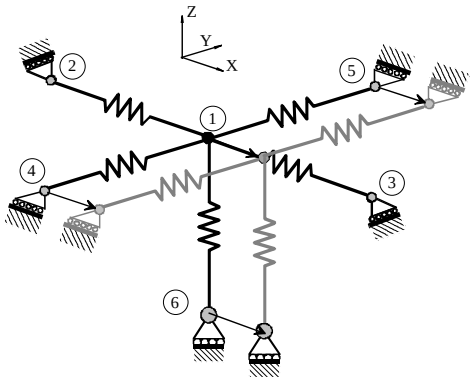

a) Nodal constraint in x-direction

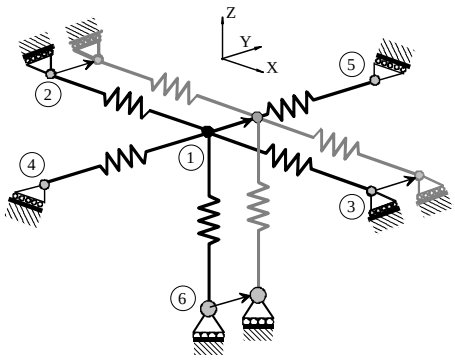

b) Nodal constraint in y-direction

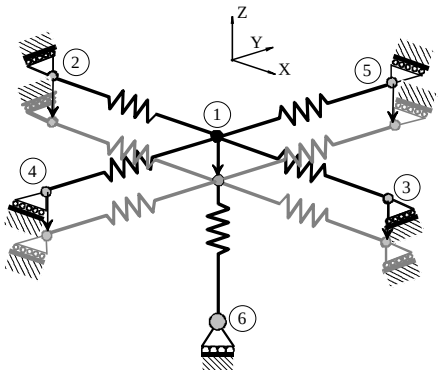

c) Nodal constraint in z-direction

Figure 5.17 Nodal constraints in three global directions

5.6 Soil-Cap interaction Model of Pier-1 in LS-DYNA

Recognizing the importance of buried cap and seal lateral resistance, which was discussed in the context of the experimental tests in Section 5.4, a soil-cap interaction model was incorporated into the Pier-1 model. The model was developed and calibrated based on the soil response experimentally measured during the dynamic barge impact test program.

For simplicity, the p-y curve construction for the cap and the seal used in this study was based on the same technique that was used to construct the p-y curve for the piles. Soil in the front of cap was modeled using a collection of 20 nonlinear p-y springs arranged in 4 horizontal rows and 5 vertical columns. The rows were located at elevations -10.25ft, -11.5ft, -12.75ft, -14ft. The soil in the front of seal was modeled using 15 nonlinear p-y springs arranged in 3 horizontal rows and 5 vertical columns. The rows were located at elevations -16ft, -18ft, -20ft. For the purpose of generating p-y curves, the cap and the seal were treated as if they were composed of 5 pseudo-square piles standing side by side. The width of each of these imaginary piles was equal to 1/5 of the cap width

or seal width as appropriate. The width of pile cap and seal is the dimension perpendicular to the direction of the impact (see Figure 5.18).

The stiffness of p-y springs were calibrated such that their total force was close to the maximum static lateral resistance of the cap and seal measured during the in-situ tests. The lateral resistance soil springs were implemented in LS-DYNA using the nonlinear material model called `*MAT_SPRING_NONLINEAR_ELASTIC`. For this model, the loading curve and unloading curve are the same. This spring material model was chosen because during dynamic impact, a gap between the soil and cap interface does not form due to the sandy soil behavior as discussed above. A similar configuration of nonlinear springs was also incorporated into the model to represent the resistance provided by the soil at the back of the cap/seal.

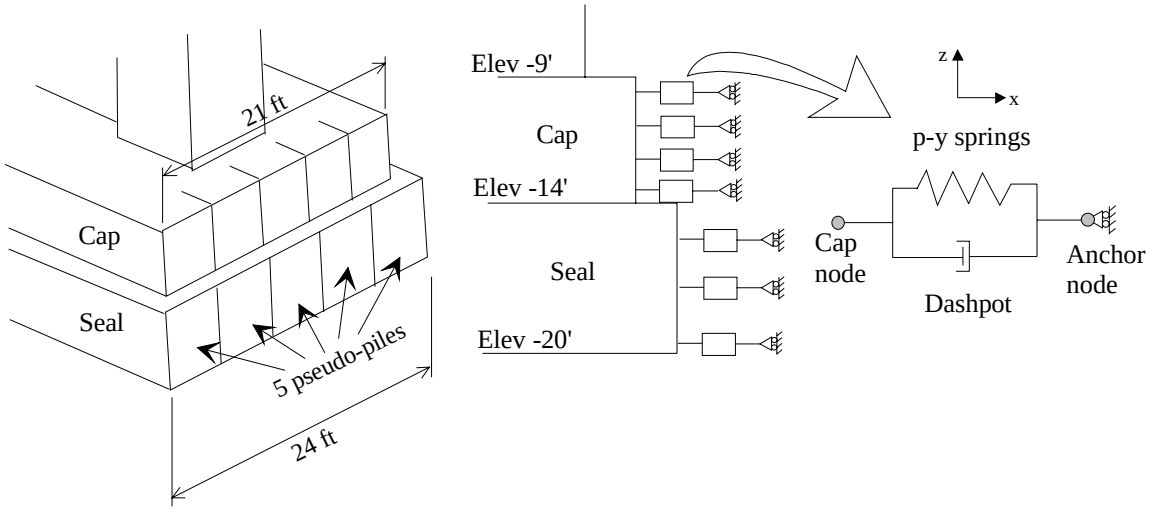

Figure 5.18 Lateral cap-soil interaction model

To account for the increase of soil resistance under dynamic loading and energy dissipation through radiation damping, linear dashpot elements parallel to the p-y springs

are incorporated in the soil-cap interaction model (Figure 5.18). Damping values may be estimated using Equation 5.1 (NCHRP Report 461):

$$C = 2D\frac{\gamma}{g}(v_s + v) \tag{5.1}$$

where C is the damping value (the force per unit length of the pile, or height of the cap and seal) is obtained by multiplying C with the velocity of the pile); D is diameter of the pile (or width of the cap or seal); g is the acceleration of gravity; v_s is the shear wave velocity of the soil; γ is the unit weight of the soil; v is the average shear wave and compression wave velocity of the soil.

However, using damping values calculated from the Eqn. 5.1, simulation results showed that the total damping force was about 400kips. From Figure 5.9 , the experimentally measured total damping force was about 120kips. Calibration of the model to the test data then required that one quarter of damping value calculated from Eqn 5.1 be used for the dashpots in the model.

Similar to the pile soil springs discussed earlier, the anchor node for each spring and dashpot set was constrained to move with the corresponding cap/seal node in the y and z direction to ensure the horizontal alignment in x-direction of the spring and dashpot (Figure 5.18).

Soil-cap interaction modeling also required additional considerations regarding soil stiffness loss that occurs during cyclic dynamic loading. Such stiffness degradation is generally attributed to the effect of repetitive remolding of the soil. When the cap/seal of Pier-1 moves, the soil in the active zone is disturbed. The sandy soil tends to follow the movement of the cap/seal filling in the newly created gap. When the cap/seal moves in reverse direction, the passive zone gradually becomes the active zone and the soil in the

current active zone is also remolded. Hence, when the soil is subjected to cyclic loading, loss of soil stiffness must be taken into account (Figure 5.19).

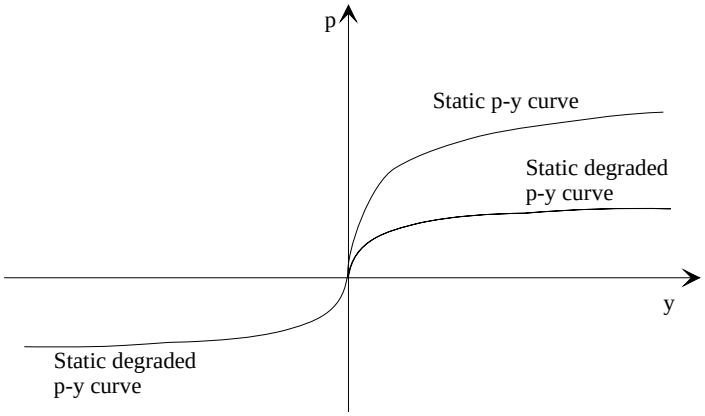

Figure 5.19 Cyclic degradation of soil due to remolding

Currently, LS-DYNA does not have a spring material model available that is directly capable of representing cyclically degrading behavior. To approximate such behavior, a modification was made to the soil model by replacing each original p-y spring by two separate component-springs having complimentary characteristics. Splitting of the load-deformation curve into component springs is illustrated in Figure 5.20.

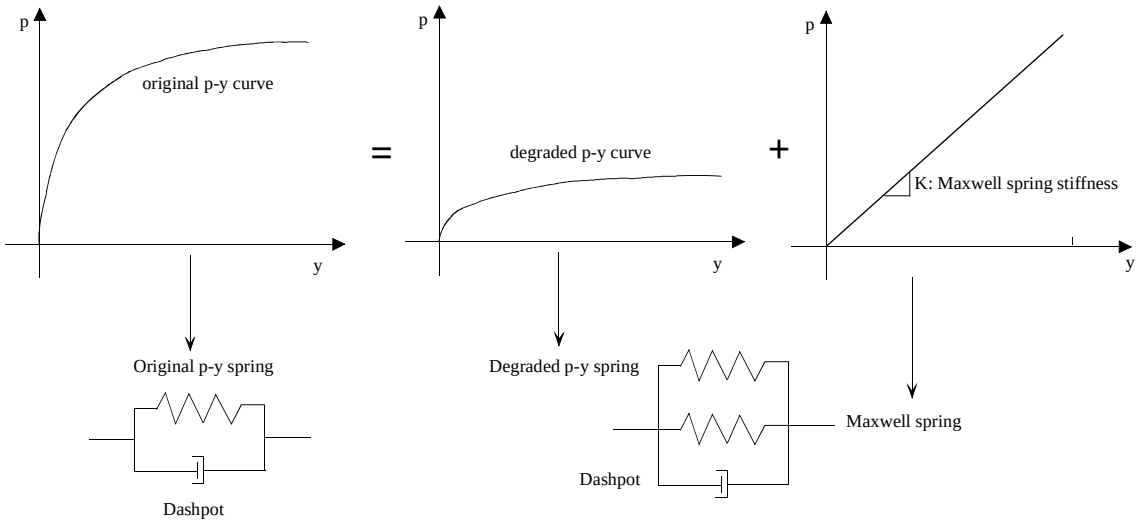

Figure 5.20 Soil model for cyclic degradation

Ideally, it would be desirable to split the overall p-y stiffness of the soil (left part of Figure 5.20) into two components each having a shape similar to that of the overall curve but reduced in magnitude. After completion of one cycle of deformation, the contribution of one of the component springs could be terminated leaving only the effect of the "degraded" spring (center part of Figure 5.20). Presently, however, LS-DYNA does not feature a *nonlinear* inelastic spring material model that permits the contribution of an element to be "terminated" after a given number of cycles or a given amount of elapsed time. However, one of the linear load-deformation spring material models, `*MAT_SPRING_MAXWELL`, does permit specification of a termination time - a time after which the effect of the element is removed from the analysis. Thus, as a trade-off, this linear material model (right part of Figure 5.20) is used to approximate the portion of the initial soil spring stiffness that needs be degraded (terminated) after the first cycle of loading.

The termination time for the linear spring was specified as 0.45 sec since this was the experimentally measured duration of time required for the pier to go through one complete cycle of displacement. After 0.45 sec, the linear spring carries zero force and only the degraded nonlinear spring is in effect for the second and following cycles of oscillation.

The extent of p-y curve degradation depends on many factors including properties of soil, variation and rate of loading, width and height of the cap/seal, and pile stiffness. Precise quantification soil models to account for such effects requires further research. For this study, degradation of soil stiffness was assumed to be equal on both sides (lead and trail) of the pier. As noted above, the level of degradation also does not change after

completion of the first cycle of load. Finally, the magnitude of the degraded p-y curve was taken as 30% of the original p-y curve.

5.6.1 Skin Resistance of Cap/Seal

Another important source of lateral resistance provided by the cap/seal is frictional force, or “skin” force. The cap and seal are massive concrete elements embedded in soil with the mud-line located at the top of the cap. Therefore the contribution of the resistance produced by frictional sliding between the cap/seal and the surrounding soil must be included. Frictional forces can develop along the bottom of the seal and along the two sides of the cap and seal. To model these resistances, nonlinear skin-friction springs were added to nodes on the interface between the bottom of the seal and the soil. The maximum force that each spring can mobilize is equal to the product of failure shear strength of the soil at bottom of the seal and the tributary area corresponding to the spring. Properties of these springs were be specified so that they represented all of the frictional forces that could develop on both the cap and seal during impact.

This method provides a suitably accurate and conservative approximation of the total frictional force resistance. Load-deformation curves for these springs are much like the t-z curves described early for axial pile springs. However, the skin-spring t-z curves are modeled using an elastic bilinear model with a quake at 0.1 in. (a typical value for most types of soil). When soil deformation exceeds 0.1 in., the springs offer no further lateral resistance due to a plateau in their load-deformation curve. The LS-DYNA material model `*MAT_SPRING_NONLINEAR_ELASTIC` was used to achieve this behavior. The ultimate force (plateau value) for each spring was computed by summing the ultimate shear force capacity for all frictional surfaces on the cap/seal and then dividing

by the number of springs attached at the seal bottom. The ultimate friction force was calculated by multiplying the friction surface area by the soil failure shear stress.

Similar to the fact that a rapid load rate leads to a dynamic increase in soil p-y stiffness, it is assumed here that rapid loading also leads to an increase in frictional t-z stiffness on the cap/seal. Linear dashpots were incorporated into the soil friction model to account for this effect and represent energy dissipation due to damping. Dashpots were added at the seal bottom in parallel to the skin-friction springs. Methods for quantifying the increase that occurs in skin friction resistance due to loading rate are not well established. In this study, the damping values used for the dashpots were determined through a calibration process in which characteristic simulation results (peak displacements, time-to peak, period of vibration, pile forces, etc.) were brought into an acceptable level of agreement with experimental test data.

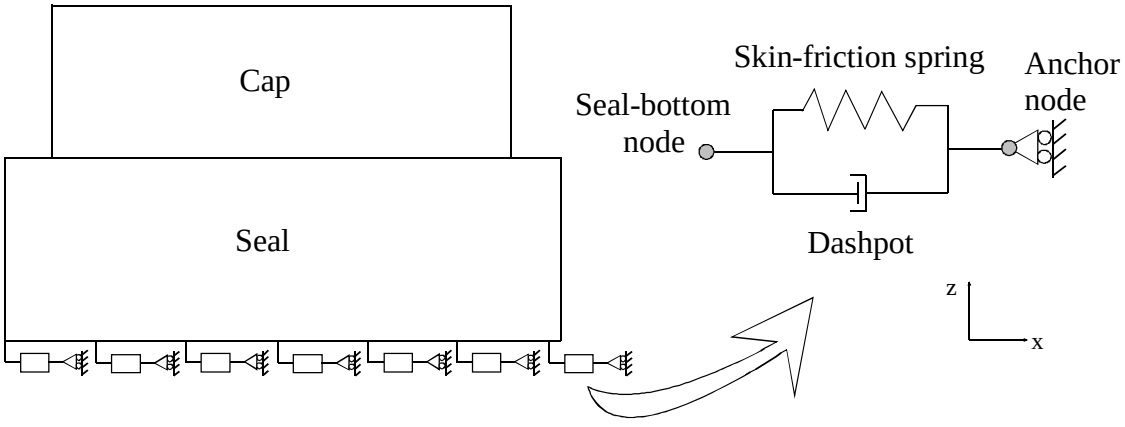

Figure 5.21 Skin-friction cap-soil interaction model

Degradation of skin-friction stiffness was also taken into account using a technique similar to that described earlier for the cap/seal p-y soil springs. The non-

degraded load-deformation t-z curve for each skin-friction spring is divided into two components (see Figure 5.22). As was the case for p-y curve degradation, the termination time for the linear portion of the skin-friction t-z spring was chosen as 0.45 sec. Further, the degraded component of the skin-friction was taken as 30% of the original curve.

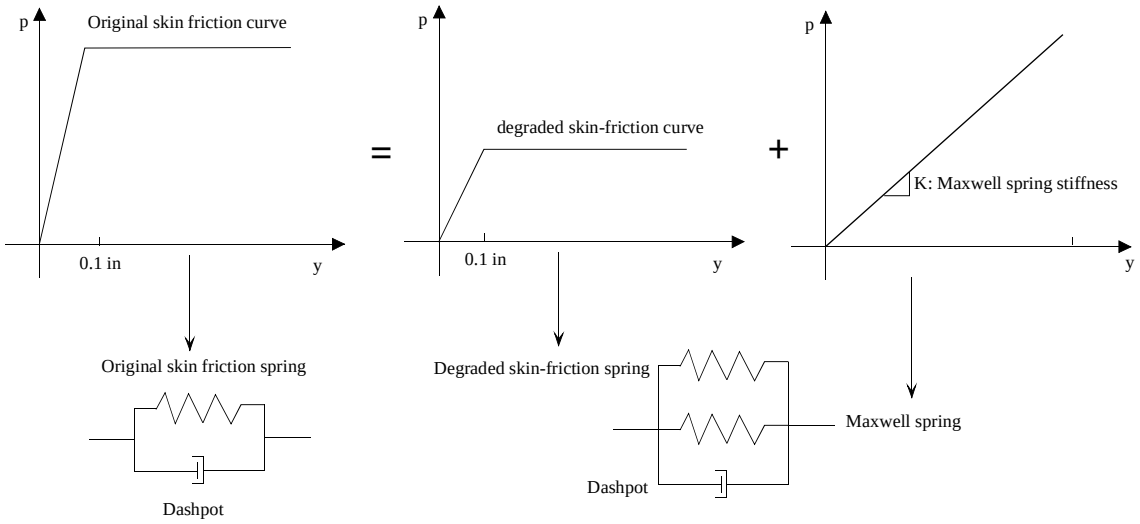

Figure 5.22 Soil model for skin friction degradation

5.7 Soil-pile Interaction Model of Pier-1 in FB-MultiPier

Soil-pile interaction in FB-MultiPier is modeled using nonlinear springs attached at the pile nodes. However, the FB-MultiPier program does not require the user to explicitly define spring elements individually as in LS-DYNA. Instead, the soil springs are implicitly incorporated into the analysis code to represent the soil reaction on the piles. Basing on user specified soil properties, the program constructs nonlinear load-deformation curves automatically. However, FB-MultiPier also permits the user to override the automatic curve calculation and define custom (“user-specified”) load-deformation curves. In order to build confidence in the fidelity of both the

LS-DYNA and FB-Multipier analysis results, it was a goal of this study to try to match analytical results obtained from these codes not only to each other, but also to the experimentally collected data.

Lateral spring behavior in the FB-Multiper model was characterized using p-y load-deformation curves. Applying the same approach used in LS-DYNA, from the pile top to elevation -32 ft, dynamic p-y curves were incorporated into FB-MultiPier through specification of user-defined p-y curves. From elevation -32 ft downward, FB-Multipier was permitted to automatically compute the (static) p-y curves. For sandy soil, FB-MultiPier offers two methods for static p-y curve construction: the O'Neill method and the Reese, Cox and Koop method. For consistency with the method used in LS-DYNA, the Reese, Cox and Koop method was chosen. For clayey soil layers, the Matlock method for "soft clay in the presence of water" was used. Dynamic p-y curves were defined at the top and bottom of each soil layer within the pile head zone. FB-Multipier interpolates the curves at pile node elevations within the layers. To prevent the problem of assuming zero lateral spring stiffness whenever pile displacement at a pile node exceeded the maximum displacement from the measured dynamic p-y curves, the dynamic p-y curves were extended to accommodate displacements of up to 1inch as in LS-DYNA (see Figure 5.14). Pile group effects were included in the model using the same p-multiplier values used in LS-DYNA. For axial soil springs on the piles, FB-Multipier automatically computes t-z curves using the method developed by McVay et al. (1989) for driven piles.

5.8 Soil-Cap/Seal Interaction Model of Pier-1 in FB-MultiPier

Currently, FB-Multipier represents load transfer from a pier structure to the surrounding soil only through the soil-pile interaction. Therefore, it is well suited to

applications involving pier structures where the pile cap is above ground (not buried). For buried pile cap pier structures, however, pier responses computed by FB-MultiPier will be in error unless additional modeling of the lateral soil resistance against the cap/seal is incorporated. In order to analyze Pier-1 using FB-Multipier, modifications were made to account for the embedded pile cap effects.

Because FB-Multipier models soil reactions only at *pile* nodes, some of the piles were modified so that lateral forces on the cap/seal were be represented by forces acting on the upper (embedded) portions of piles in the lead row. Cross-sections for H-piles in the lead row were defined in two distinct segments (zones) for each pile. The first segment consists of a fictitious square pile 8.5 ft in length, starting at the mid-plane of the pile cap and extending to the bottom of the seal. The cross-sectional width of this segment is 54 in - equal to the average width of the cap/seal divided by the number of piles at the lead row. This modeling approximation is much like the method used in LS-DYNA and described earlier. That is, the cap/seal resistance is equal to the total resistance of five piles standing side by side. It is noted that the length of the first segment starts from the center of the cap because the cap is modeled in FB-Multipier using flat shell elements. The second segment of each H-pile extends from the bottom of the seal to the bottom of the pile and utilizes the normal cross-sectional properties of the HP 14x73 piles (see Figure 5.23).

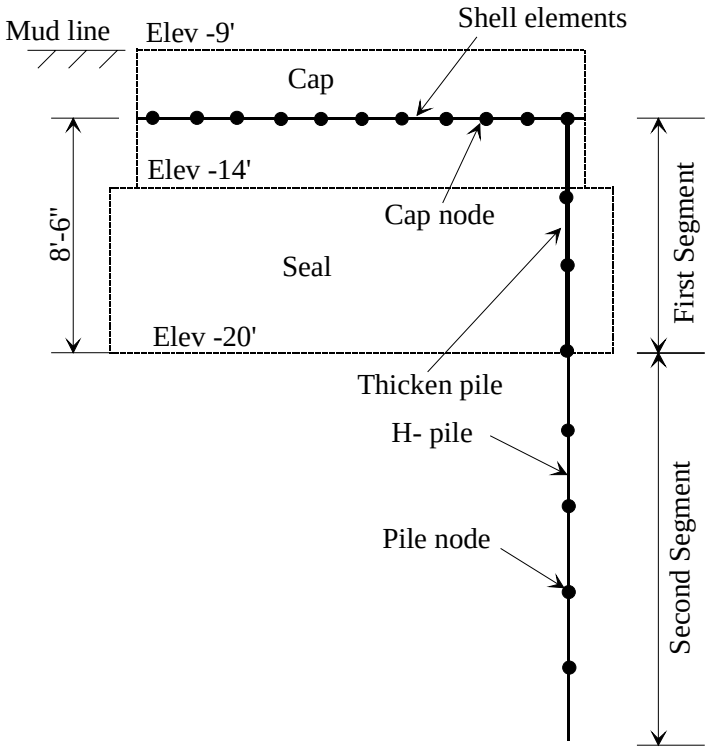

Figure 5.23 Modification of H-pile (Lead row)

When the pile cap is embedded, the pile nodes of H-piles other than lead row piles lying between the center of the cap to the bottom of the seal still have the soil reactions acting on them. Care must be taken in modeling these soil reactions because if the cap/seal has only lateral soil reactions on the front and back sides, the model will over estimate the resistance of the cap/seal. However, since the cap/seal also has skin friction acting on two sides, on the top and bottom of the seal, the total of soil reaction on these pile nodes are assumed equal to the skin friction forces acting on the cap/seal. Soil stiffness degradation during impact of all p-y springs that represent the forces acting on the cap/seal are specified with the degraded soil factor of 0.3. Also, as in LS-DYNA, p-y springs that represent the soil reaction on the cap and seal are specified as being a no-gap soil model.

The increase of soil resistance under dynamic loading and the energy dissipation through radiation damping are represented in the FB-Multipier model by introducing 13 dashpots on the cap nodes (see Figure 5.24). The total damping value used for FB-Multipier dashpots is computed by summing the damping values of all dashpots in LS-DYNA model. The “summed damping value” approach is used with the assumption that the pier displaces laterally only with negligible rotation as seen in experimental results.

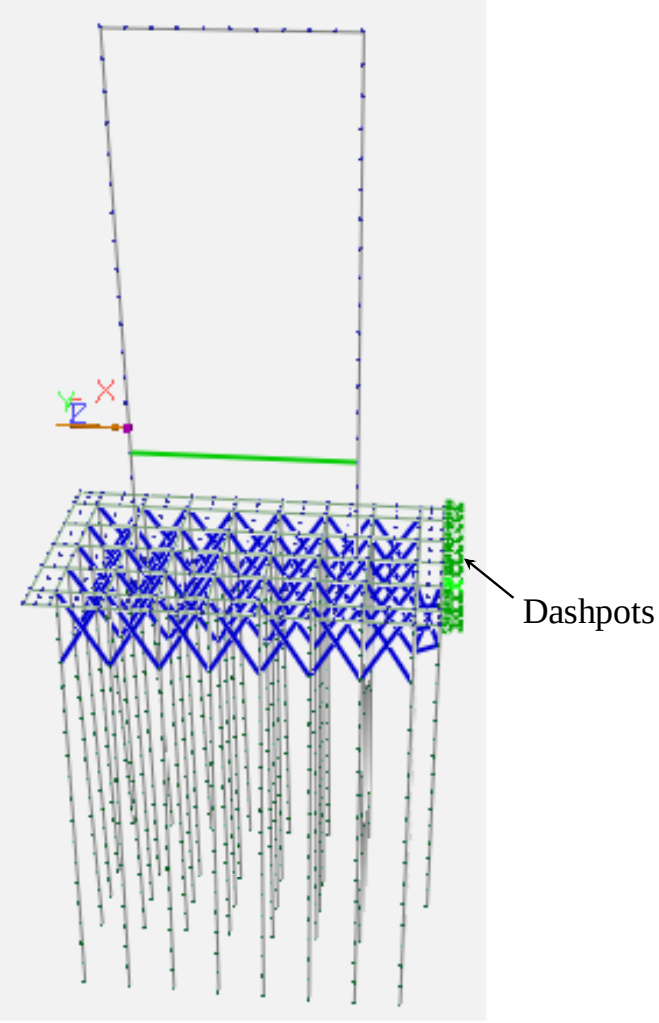

Figure 5.24 Dashpot in the FB-Multipier model

CHAPTER 6
CALIBRATION AND ANALYSIS OF NUMERICAL MODELS

6.1 Discussion of P1T7 Experimental Results

Impact test P1T7 (Pier-1, Test-7, see Consolazio et al. 2005 for additional details) was a high-energy barge-pier collision test producing an impact load of 864 kips and significant barge deformation. The barge velocity was 3.41 knots (5.74 ft/sec) which generated a kinetic impact energy of 622 kip-ft. A time-history of impact force measured during the test is presented in Figure 6.1. A corresponding time-history of pier displacement at the impact point is plotted in Figure 6.2. Shear force measured in an instrumented pile attached to the pier is shown in Figure 6.3. In order to understand the correlation among impact load, pile head shear force, pier displacement and soil reaction, normalized plots of the above parameters are presented in Figure 6.4.

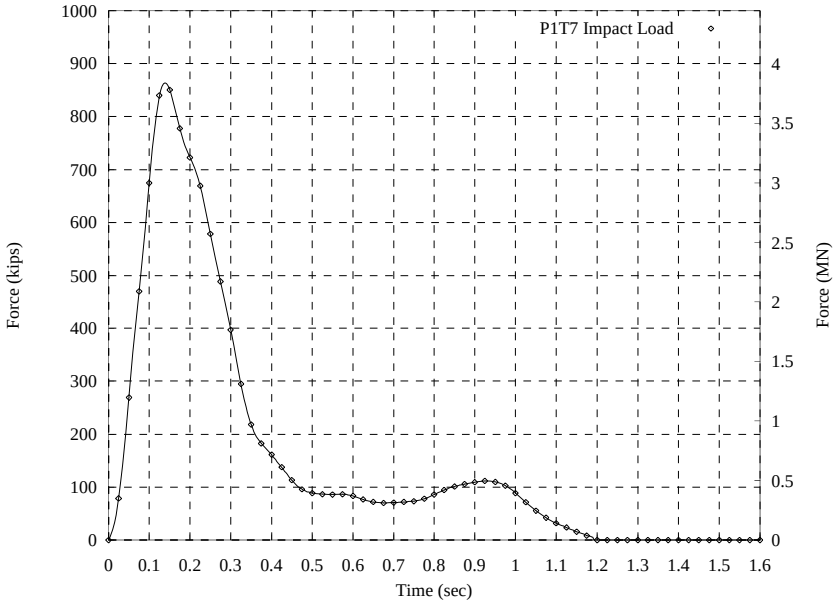

Figure 6.1 Impact load for test P1T7

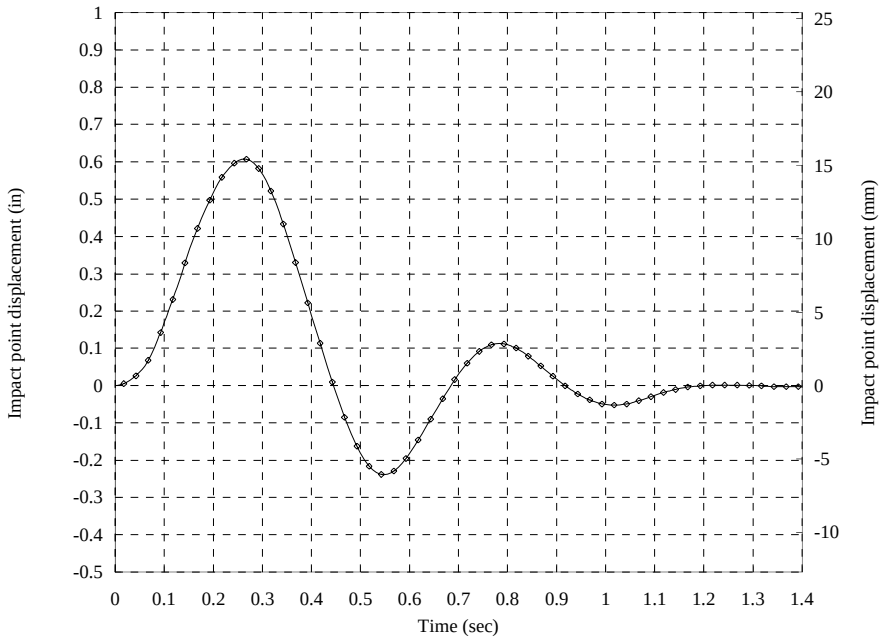

Figure 6.2 Impact-point displacement for test P1T7

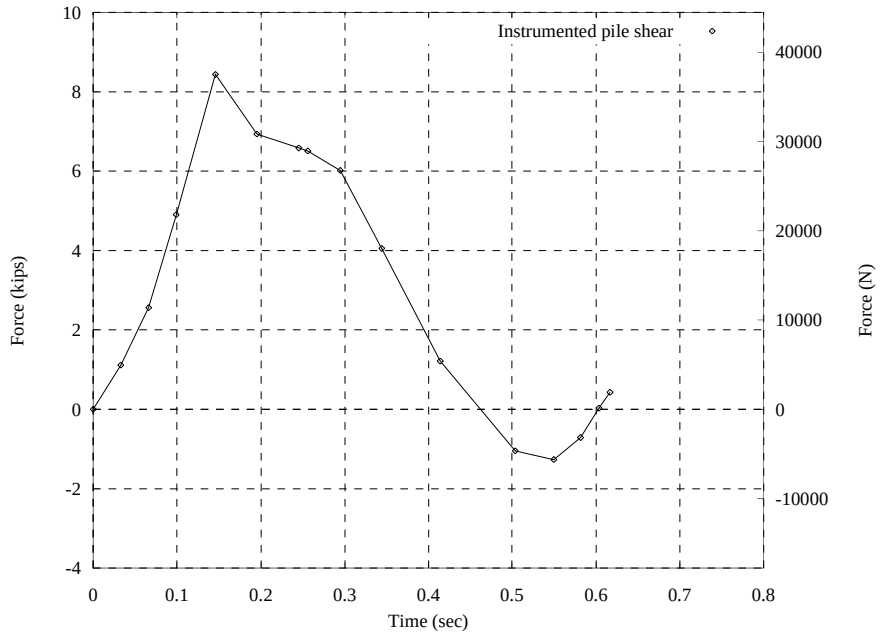

Figure 6.3 P1T7 instrumented-pile shear

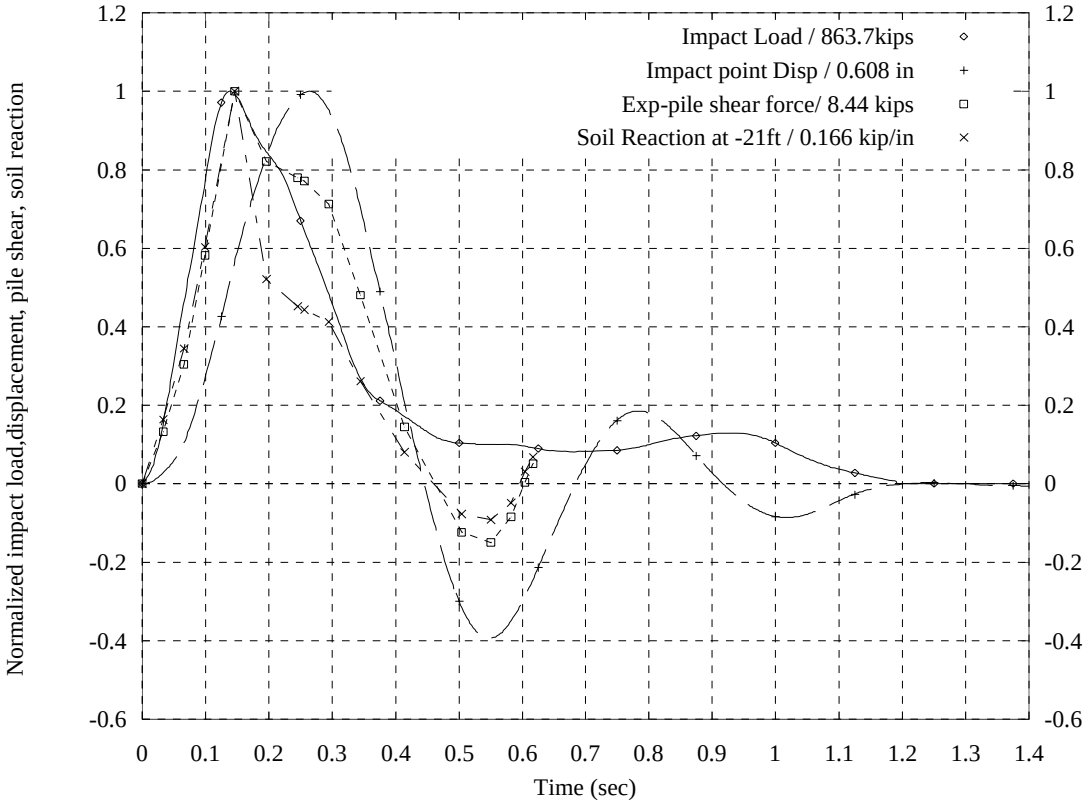

Figure 6.4 Normalized test data

Figure 6.4 reveals that the pile shear force and soil reaction at the pile head peaked at the same time (t=0.15 seconds), which was expected. Maximum velocity occurred at approximately this same point in time (as indicated by the slope of displacement curve), thus dynamic rate-dependent components of soil resistance maximized at this same point in time. As the velocity decreased from 0.15 to 0.25 sec, the dynamic component of soil resistance decreased. Thus, even though displacements continued to increase from 0.15 to 0.25 sec, the pile shear actually decreased slightly during this timeframe. The fact that maximum pile shear force did not occur at the point of maximum pile head displacement is a very clear indication of the presence of dynamic phenomena.

6.2 Calibration of Analysis Models with Experimental Data

Applying the time-varying impact loads measured during test P1T7 (Figure 6.1) to LS-DYNA and FB-Multipier models of Pier-1, numerous parametric analyses were conducted to investigate sources of both static and dynamic resistance and to calibrate the models. As a result of this process, model components were included to account for resistance of the cap/seal, dynamic soil behavior including rate-effects and damping, and soil stiffness degradation.

Comparisons of pier displacements at the impact point obtained from calibrated LS-DYNA and FB-Multipier models and experimental testing are presented in Figure 6.5. Pier displacement time-histories compare well and all achieve nearly the same peak value and time-to-peak. Pier motions during the most dominant forced-vibration portion of the loading history, from zero to approximately 0.5 sec (see Figure 6.1), are in good agreement. This indicates that the level of structural demand on the pier and foundation is well represented during the most important portion of the collision.

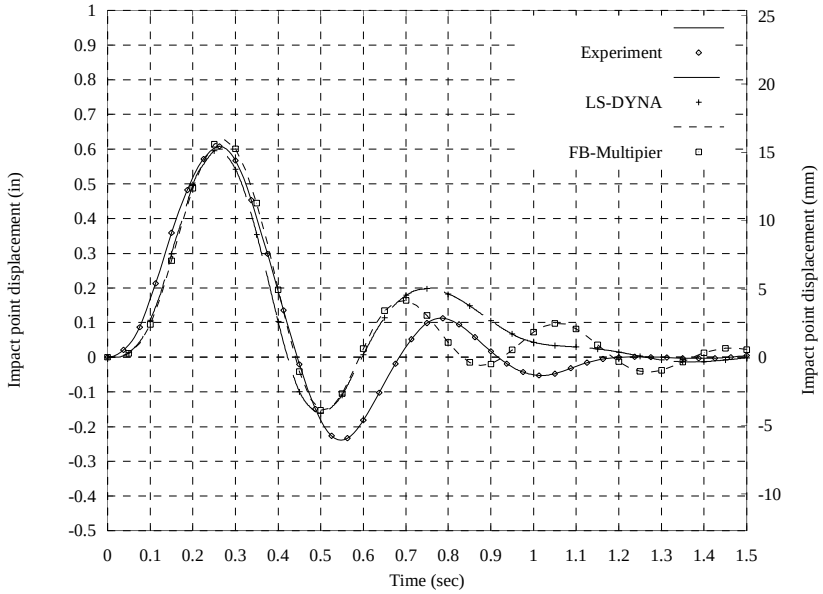

Figure 6.5 Time history of pier displacement

Of equal importance in validating the pier/soil modeling procedures is the ability to predict pile shears, pile deflected shape, and forces acting on the cap/seal that agree with experimental results. The shear force time-history measured by an instrumented-pile in the experimental tests is compared to data computed by LS-DYNA and FB-Multipier analyses in Figure 6.6. Good agreement is observed with regard to shear magnitude and periodicity. A related parameter of interest in design is the total shear force generated by all piles in the foundation system. Experimental data was collected only for a single instrumented pile. However, the numerical models can be used to assess total pile forces as shown in Figure 6.7. Maximum total shear forces predicted by LS-DYNA and FB-Multipier are in good agreement and average around 275 kips. In comparison to the magnitude of the 864 kip impact load, the total pile shear constitutes an important component of pier resistance (as is well understood in pier design). It should be noted that since pile group effects were incorporated into the model, each row of piles contributed differently to the shear total. Figure 6.8 and 6.9 illustrate the variation in shear for different pile rows as computed by LS-DYNA and FB-Multipier respectively.

In order to compare pile deflections predicted analytically and measured experimentally, deflected shapes for the instrumented-pile at the point of maximum pile displacement are presented in Figure 6.10. Reasonable agreement between simulation and experiment is indicated, implying a suitable representation of pile-soil resistance forces in the numerical models. Observed differences are primarily attributable to differences in numerical model resolution and the nodal locations at which the soil springs are incorporated in the models.

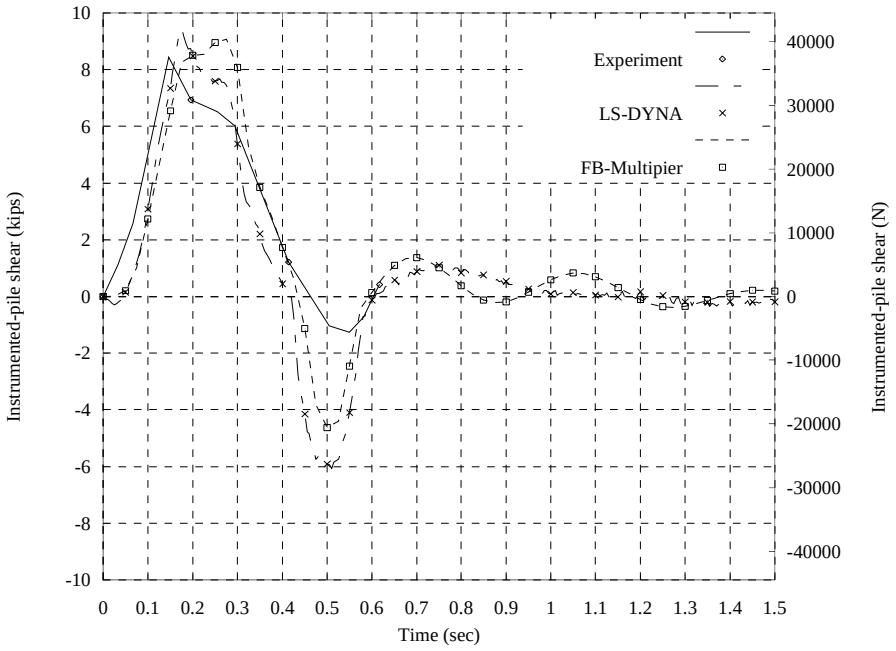

Figure 6.6 Time history of instrumented-pile shear

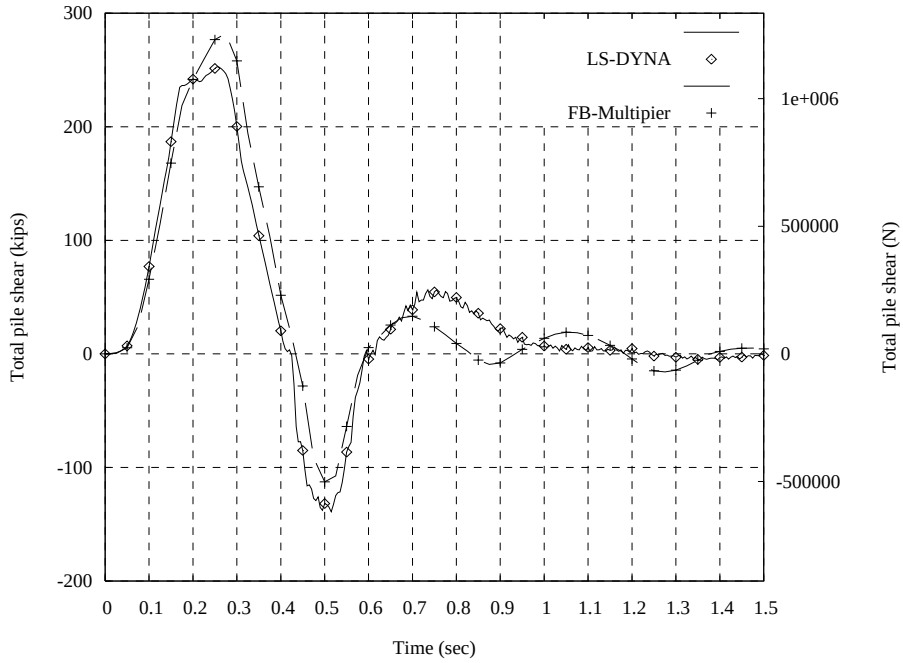

Figure 6.7 Time history of pile shear total

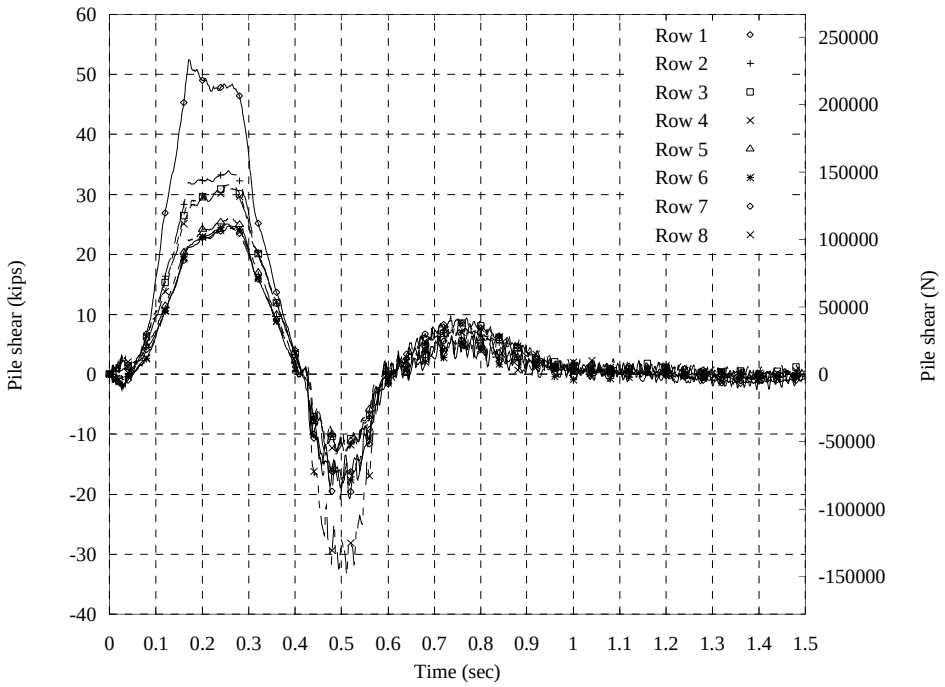

Figure 6.8 Time history of pile shear by row (LS-DYNA)

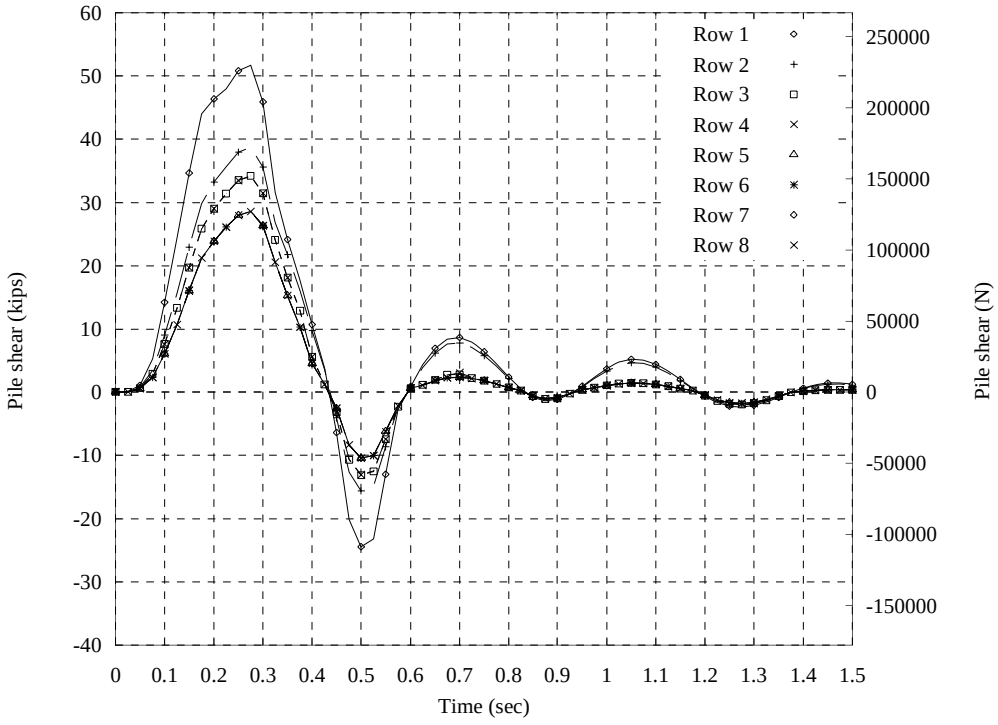

Figure 6.9 Time history of pile shear by row (FB-Multipier)

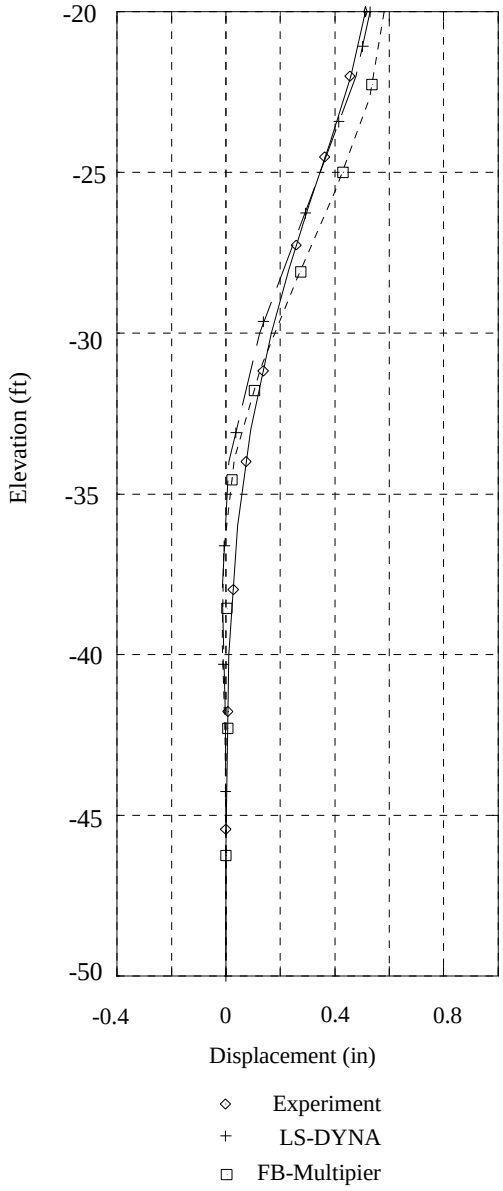

Figure 6.10 Pile deflection at maximum displacement

Further model validation involves comparisons of soil forces acting on the cap/seal. Shown in Figure 6.11 are resultant forces (passive and active soil forces) acting on the front (lead) and back (trail) sides of the cap/seal. It must be noted that the forces

plotted are the total of both static and dynamic soil resistance. To understand the contribution of each type of resistance, separate “static” soil forces represented by springs and “dynamic” soil forces represented by dashpots from LS-DYNA and FB-Multipier analyses are shown in Figure 6.12 and 6.13. Time histories of spring forces and dashpot forces predicted by both LS-DYNA and FB-Multipier compare well. It should be noted that the spring forces and dashpot forces peak at different points in time. While the spring forces peak at the time of maximum pier displacement, dashpot forces peak earlier at a point in time corresponding to the maximum pier velocity.

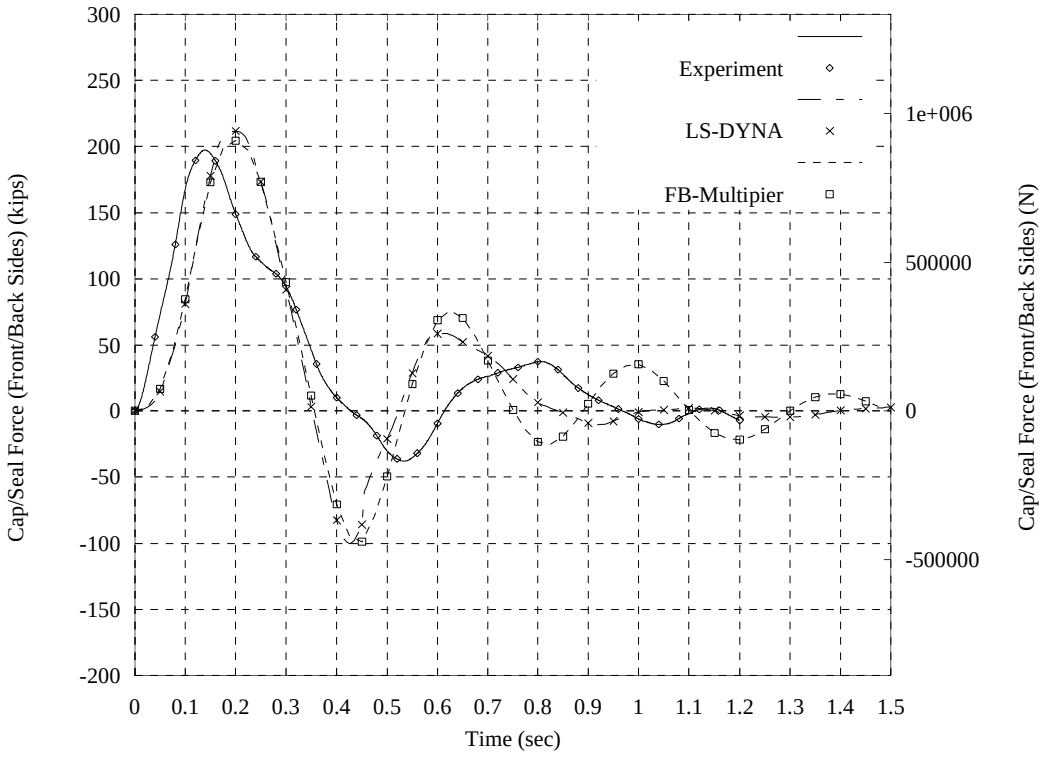

Figure 6.11 Time history of soil force acting on front and back of pile cap/seal

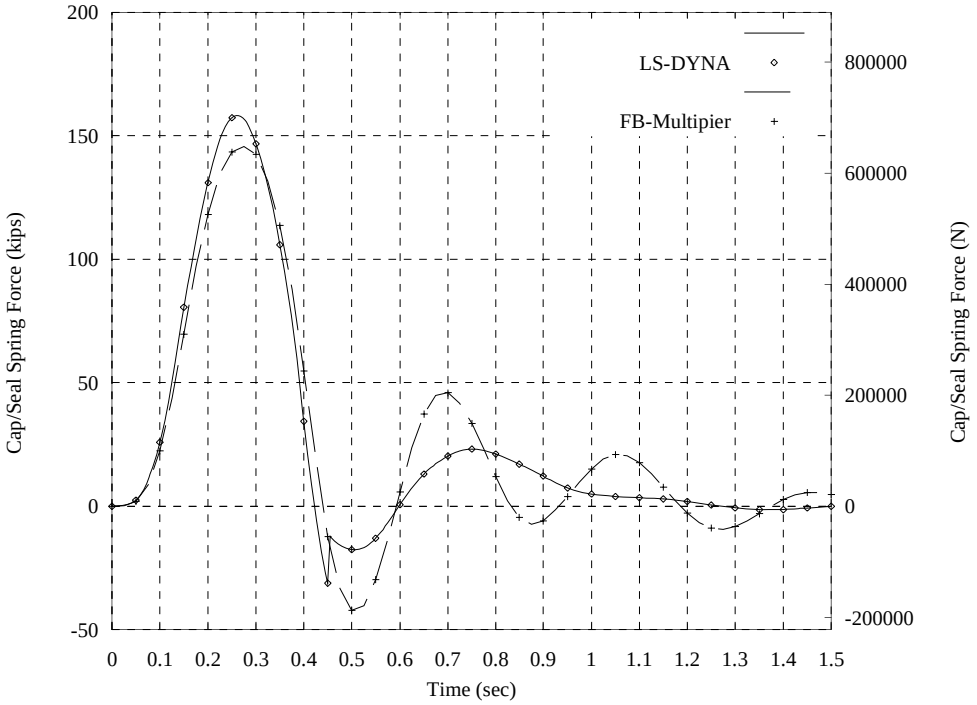

Figure 6.12 Time history of static soil force acting on front and back of pile cap/seal

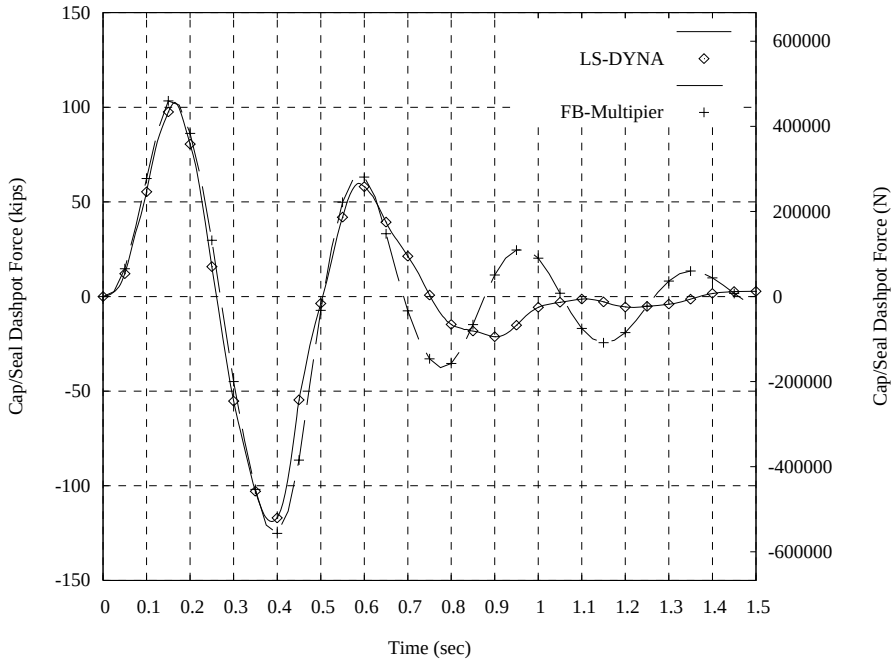

Figure 6.13 Time history of dynamic soil force acting on front and back of pile cap/seal

In addition to soil forces acting at the front and back faces of the cap/seal (p-y resistance), skin friction t-z forces acting on the sides and bottom of the cap/seal are also of interest. Skin forces include both static and dynamic components of resistance. Total skin forces (dynamic plus static) are presented in Figure 6.14. Generally, the two predictions are in reasonable agreement. The most noticeable differences are attributable to differences in the techniques used in LS-DYNA and FB-Multipier to model cyclic degradation of soil stiffness. Recall from Chapter 5 that in the LS-DYNA model, linear soil springs with a termination time of 0.45 sec. were used to approximate degradation of soil stiffness after completion of one cycle of loading. The abrupt change in the LS-DYNA skin force trace in Figure 6.14, occurring at 0.45 sec., is an artifact of this approximate method of modeling degradation. In the future, a more sophisticated LS-DYNA model of degradation needs to be developed. In Figure 6.15 and 6.16 time histories of the skin spring force (static resistance) and skin dashpot force (dynamic resistance) are presented.

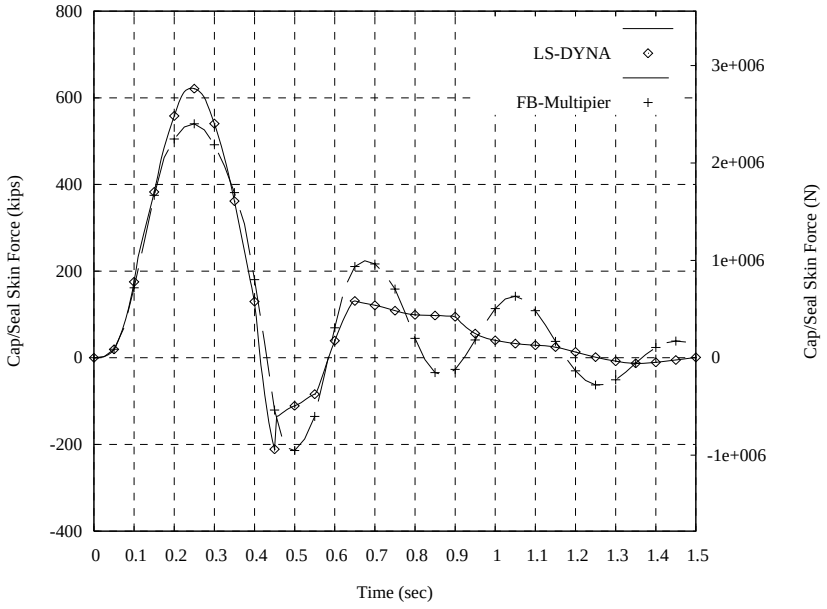

Figure 6.14 Time history of total soil skin force acting on pile cap/seal

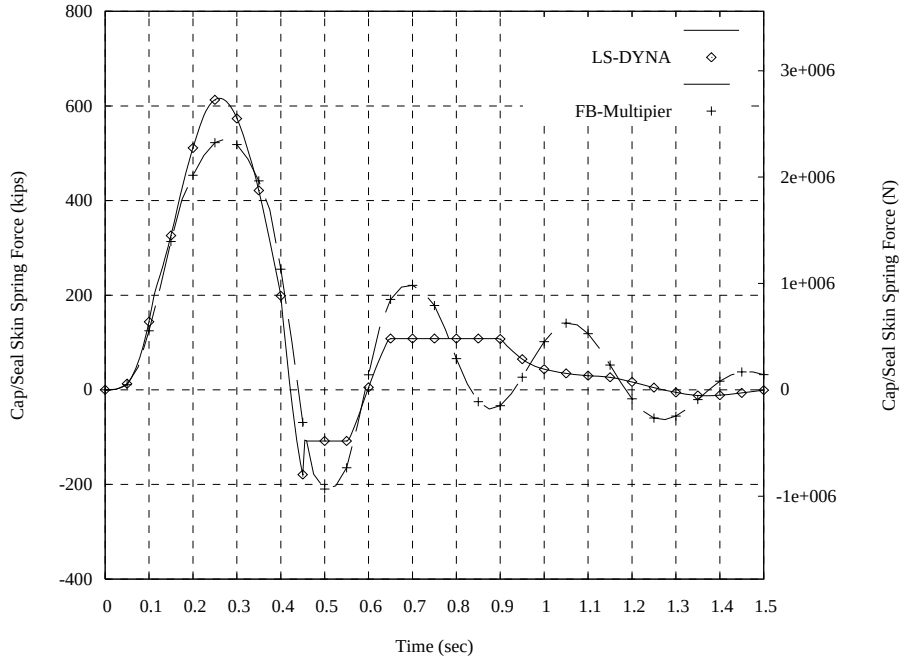

Figure 6.15 Time history of static soil skin force acting on pile cap/seal

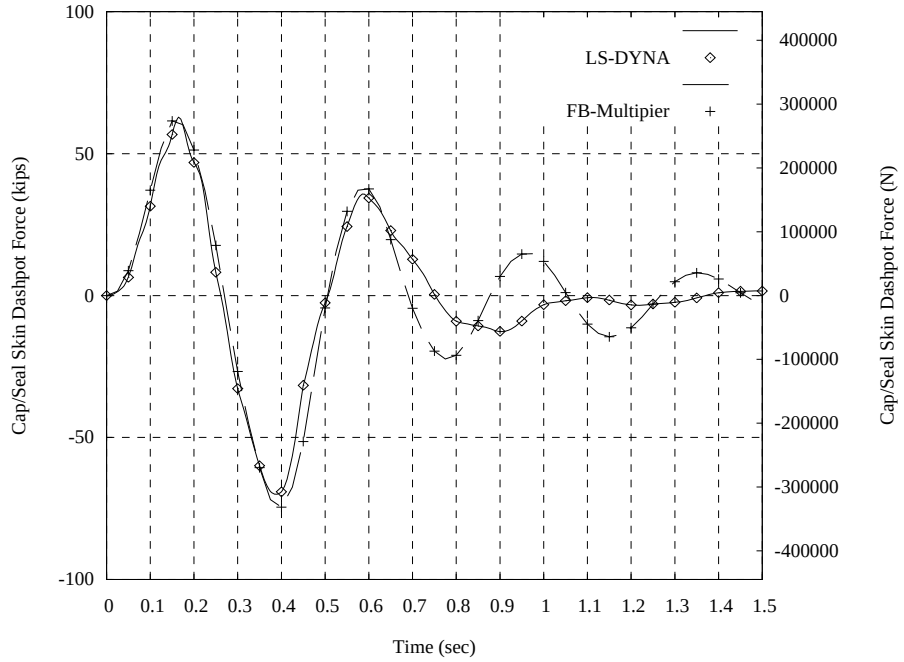

Figure 6.16 Time history of dynamic soil skin force acting on pile cap/seal

To complete the discussion of impact loads and sources of resistance, consideration is now given to inertial (mass-related) and structural damping forces in the pier. Forces acting on the pier during a collision include the impact force, pile shears, soil p-y forces on front and back of the cap/seal, soil skin t-z forces on cap/seal, inertial forces on the pier, and structural damping forces on the pier (see Figure 6.17). Based on equilibrium of forces acting on the pier, the sum of the structural inertial and structural damping forces can be determined. In Figure 6.18, time histories of this force-quantity are plotted. Note that both of the components of this quantity—inertia and damping—would be zero for a static loading condition in which there is no acceleration or velocity. Thus this quantity provides measure of the influence of purely dynamic forces acting on the structural portion of the pier (pier bent, pile caps, etc.). Comparing the force magnitudes in Figure 6.18 to the peak applied force of 864 kips, it is noted that dynamic structural sources of resistance are, as in the case of dynamic soil effects, on the same order of magnitude as the applied loading and therefore not negligible.

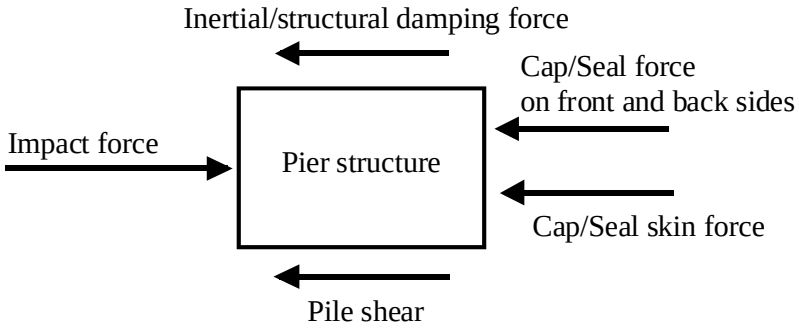

Figure 6.17 Schematic of forces acting on the pier

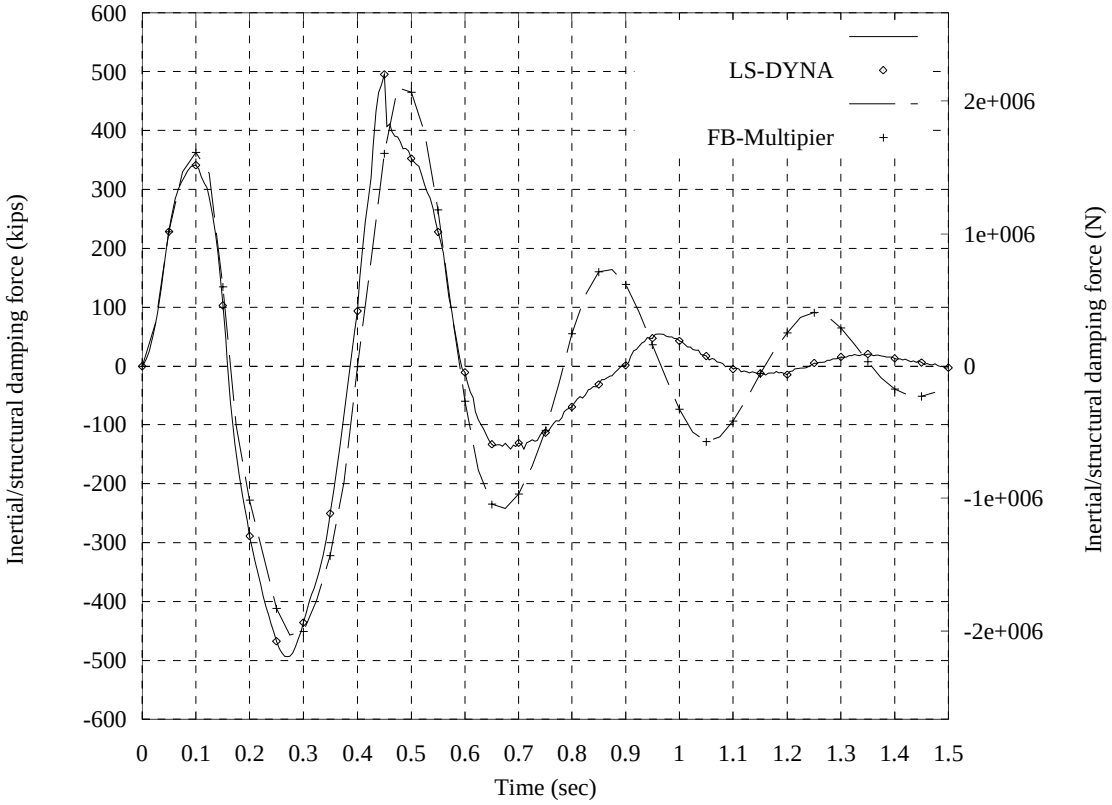

Figure 6.18 Time history of pier inertial/structural damping force

6.3 Comparison of Dynamic and Static Analysis Results

Present, bridge pier design procedures for barge impact loading utilize static load calculation procedures (the AASHTO barge impact provisions) and static (linear or nonlinear) structural analysis techniques. In this section, comparisons are made between structural demands computed via static procedures and corresponding structural demands computed using dynamic analysis procedures. For the static analyses, a static FB-Multipier model of Pier-1 was constructed by removing all dashpots from the dynamic FB-Multipier model described earlier and replacing the field-measured dynamic p-y curves with corresponding static p-y curves (i.e., the dynamic increases in soil

resistance measured during P1T7 were removed from the p-y curves). Static loads were then applied to the pier model and nonlinear static analyses were performed.

Two separate static load cases were evaluated for this portion of the study. During test P1T7 at St. George Island, the peak dynamic load measured (see Figure 6.1) was 864 kips. In the first static load case analyzed, the peak 864 kip load is applied to Pier-1 as a static (infinite duration) load. Comparisons between structural demand indices obtained from this analysis, versus similar results obtained from a dynamic FB-Multipier analysis for the load history of Figure 6.1, permits a direct evaluation of the differences between static and dynamic structural assessment. In addition, a second static load case was also considered in which the impact energy for test P1T7 was used in conjunction with the AASHTO barge impact provisions to compute a static-equivalent impact load. The resulting static load, for which calculation details are given in the Appendix, was 1968 kips.

Key results from the static and dynamic analysis cases are summarized in Table 6.1. A comparison of cases A and C permits a comparison of static and dynamic analysis for matched pier, soil, and load magnitude. The dynamic analysis predicted a pier displacement of 0.627 in. whereas the static analysis predicted a displacement of 0.475 in. In this case, because the duration of the dynamic loading pulse was close to the natural period of the structure, there was an increase in displacement beyond that predicted by static analysis. Similarly, the H-pile shears predicted by dynamic analysis were larger than those predicted by static analysis—10.3 kips dynamic; 8.4 kips static.

In contrast, an examination of the maximum pier column shear forces reveals that the dynamic analysis predicted a noticeably lower shear force than the static analysis—

539 kips dynamic; 856 kips static. Similarly, if the pier column failure ratio is examined, it is noted that the dynamic analysis predicted a less severe combined-axial-moment demand-to-capacity ratio—0.25 dynamic; 0.34 static. The conclusion to be drawn from comparing cases A and C is that it cannot easily be determined whether static analysis procedures are conservative or unconservative. The results here indicate that use of a static analysis to assess response to a dynamic loading condition will lead to a mixture of conservative and unconservative predictions. The exact mixture of which demand indices are conservative and which are unconservative depends heavily on the characteristics of the vessel, the pier structure, and the soil properties. Dynamic analysis offers a rational means of evaluating structural demand indices throughout the structure without having to substantially increase the target static design load levels to ensure sufficient safety.

Comparing cases A and B, it is noted that following the current AASHTO static design provisions leads to conservative, but uneconomical results. The pier displacement predicted using the AASHTO load is nearly an order of magnitude larger than that predicted using the actual (experimentally measured) load for the same impact energy level. Not surprisingly, the H-pile failure ratio for the AASHTO load case (1.26) indicates that the steel piles are not capable of carrying the applied load (ratio > 1.0). While the AASHTO static analysis case is conservative relative to dynamic analysis, it also has the potential to lead to severely uneconomical designs.

Table 6.1 Comparison of static and dynamic analysis results

A) Static analysis (Peak P1T7 load, 864 kips)			**B) Static analysis (AASHTO load, 1968 kips)**		
Pier Displacement	0.475	in	Pier Displacement	3.99	in
Pile top displacement	0.424	in	Pile top displacement	3.83	in
Total pile shear	226	kips	Total pile shear	1155.3	kips
Cap/Seal Soil Passive Force	116	kips	Cap/Seal Soil Passive Force	246.7	kips
Cap/Seal Skin Force	522	kips	Cap/Seal Skin Force	566.2	kips
Instrumented Pile			***Instrumented Pile***		
Shear	7.48	kips	Shear	30.79	kips
H-Pile			***H-Pile***		
Shear	8.4	kips	Shear	42.73	kips
Failure ratio	0.19		Failure ratio	1.26	
Pier column			***Pier column***		
Shear	856	kips	Shear	1950.2	kips
Moment	2745	kip-ft	Moment	6351.2	kip-ft
Failure ratio	0.337		Failure ratio	0.744	

C) Dynamic analysis (FB-Multipier) (P1T7 time history load)			**D) Dynamic analysis (LS-DYNA) (P1T7 time history load)**		
Pier Displacement	0.627	in	Pier Displacement	0.608	in
Pile top displacement	0.583	in	Pile top displacement	0.529	in
Total pile shear	282	kips	Total pile shear	251	kips
Cap/Seal Soil Passive Force	204	kips	Cap/Seal Soil Passive Force	211	kips
Cap/Seal Skin Force	540	kips	Cap/Seal Skin Force	622	kips
Instrumented Pile			***Instrumented Pile***		
Shear	9.0	kips	Shear	9.5	kips
H-Pile			***H-Pile***		
Shear	10.3	kips	Shear	10.5	kips
Failure ratio	0.24				
Pier column					
Shear	539	kips			
Moment	1960	kip-ft			
Failure ratio	0.26				

CHAPTER 7
CONCLUSIONS AND RECOMMENDATIONS

Nonlinear static and dynamic FB-MultiPier and dynamic LS-DYNA numerical models of Pier-1—an impact resistant pier of the old St. George Island Causeway Bridge—have been created and calibrated through the use of full-scale experimental barge impact test data. In both the static and dynamic loading regimes, significant sources of resistance not typically relied upon in bridge pier design have been identified and quantified through comparisons of numerical modeling results and physical test data.

In piers that employ buried (soil-embedded) pile caps, it has been found that static and dynamic soil forces acting directly on the pile cap—and, if present, the tremie seal—are as significant in magnitude as the forces that act on the foundation piles (the typical source of soil resistance relied upon in pier design practice). In the static regime, soil forces normal to the lead side of the pile cap/seal, denoted “cap/seal p-y static resistance”, are on the same order of magnitude as the “pile p-y static resistance” traditionally associated with soil resistance generated on piles. Moreover, on the longitudinal surfaces of the cap/seal, i.e. the side and bottom surfaces oriented parallel to the direction of load, soil skin-friction shear stresses have also been found to play an important role in resisting load. This source of resistance, denoted “cap/seal t-z static resistance” is on the same order of magnitude as the static p-y resistance and may even exceed it in some cases.

Of equal importance to the static cap/seal soil forces, *dynamic* sources of soil resistance have also been quantified in this study. In fact, calibration of numerical models to physical test data was only possible through the development and analysis of nonlinear

dynamic finite element models of pier and soil response. The model calibration process was based on matching, within acceptable levels of tolerance, multiple measures of system response: time varying pier displacements, time varying cap/seal p-y forces, time varying pile shears, and pile deflection profiles. Only through dynamic analysis, and the introduction of new sources of soil resistance within the numerical models, could all of these response measures be brought into reasonable agreement with the physical test data.

Through conducting dynamic analyses, and evaluating soil stress data collected at St. George Island, it was determined that the rapid nature of barge impact loads may result in a dynamic increase in the resistance forces generated by the soil. This resistance appears to be primarily related to rate-effects rather than soil inertial effects (mass related effects). That is, the increase of soil resistance appears primarily related to increased soil stiffness under rapid loading (most likely due to the saturated nature of the soil), rather than mobilization of soil forces associated with soil-mass acceleration (i.e., inertial effects). Comparisons of dynamic soil stress measurements and results from in-situ soil characterization tests conducted at St. George clearly indicated that during impact, soil resistance well exceeded the static soil capacity (as determined via in-situ tests). In this thesis, these dynamic rate-effects were introduced into the numerical models as linear viscous damping elements which model not only velocity proportional increases in resistance, but also energy dissipation (damping). Only through inclusion of such elements in the dynamic models was it possible to match the experimental results. Once adequately calibrated, the numerical models were used to quantify the degree of *dynamic* resistance as compared to the *static* resistance typically relied upon in bridge design practice. Results from this process have revealed that forces associated with dynamic

rate-effects in the soil and inertial effects in the pier-structure are on the same order of magnitude as static soil forces and associated pile shears. Thus, in the future, after additional investigation, it may be possible to rely upon sources of static and dynamic resistance to impact loads that are presently ignored in pier design. Changes of this type would lead to more economical bridge foundations.

Static-equivalent load analyses (typical of bridge pier design practice) were also conducted for the purpose of comparison to dynamic analyses so that the relative levels of structural demand predicted by the two methods could be evaluated. Two different static analysis cases were performed. In one case, the peak dynamic force experimentally measured during one of the St. George Island impact tests was applied to a bridge pier model as a static force. In the second case, AASHTO's barge impact provisions were used to quantify static-equivalent load associated with the impact energy imparted to the pier during the St. George Island test of interest. The AASHTO load was then applied to a static analysis model to asses the severity of response.

Results from the first analysis suggested that dynamic analyses are better suited to accurately assessing pier response to collision loads than are static-equivalent analysis procedures. Comparisons of structural demand predicted by static vs. dynamic methods were mixed. While the dynamic analysis predicted greater pier displacement and greater pile demand than the static analysis, it also predicted less severe structural demand on the pier columns. Given the dynamic nature of collision loads, the use of dynamic analysis is a more accurate means of rationally quantifying design parameters.

Results from the second analysis case revealed that the AASHTO provisions, when combined with static analysis procedures, are conservative and over predict the severity

of structural demand placed on structural pier components. This is primarily related to the fact that the AASHTO provisions appear to over-predict the magnitude of impact force for a particular impact energy level. This issue has been discussed in greater detail elsewhere in published literature related to the St. George Island impact tests.

Having investigated both static and dynamic effects related to the response of pier structure and soil, future research efforts need to focus on quantifying dynamic properties for various types of soils (an area for geotechnical investigation) and evaluating superstructure effects and vessel-pier interaction. Evaluating the effectiveness of bridge superstructures in shedding load from an impacted pier to adjacent piers through both stiffness (static resistance) and mass (dynamic resistance) in the superstructure is a priority. In addition, with calibrated pier/soil numerical models now developed, future focus needs to also be given to vessel modeling and analysis of dynamic barge-pier interactions during collision events. Using simplified barge models, and impact load data experimentally measured at St. George Island, robust dynamic analysis methods capable of quantifying barge impact loads—and the corresponding structural responses—need to be developed. Development and validation of such models could serve as the foundation for future design procedures that do not depend on empirical static-equivalent load calculation equations.

APPENDIX
AASHTO EQUIVALENT STATIC IMPACT LOAD CALCULATION FOR ST. GEORGE ISLAND TEST P1T7

In this appendix, the AASHTO equivalent static impact load for test P1T7 is calculated using a Mathcad worksheet. This load is then used for static analysis of the Pier-1.

AASHTO - Barge impact force calculation for P1T7

Input parameters:

Barge width : $B_M := 49.5$ (ft)

Barge weight : $w_{ton} := 604$ (tons)

$$w_{tonne} := \frac{w_{ton}}{1.102311}$$

$w_{tonne} = 547.94$ (tonnes)

Barge velocity : $V_{knots} := 3.41$ (knots)

$V := V_{knots} \cdot 1.6878$ (ft/s)

$V = 5.755$ (ft/s)

Hydrodynamic mass coefficient: $C_H := 1$

Load calculation:

Barge kinetic energy:

$$KE := \frac{C_H \cdot w_{tonne} \cdot V^2}{29.2}$$

$KE = 622$ (kip-ft)

Barge bow damage depth: a_B (Equation 3.13-1)

$R_B := B_M \div 35$

$$a_B := \left[\left(1 + \frac{KE}{5672}\right)^{0.5} - 1\right] \cdot \left(\frac{10.2}{R_B}\right)$$

$a_B = 0.385$ (ft)

Barge collision force on pier-1: P_B (Equation 3.12-1)

$$P_B := \begin{cases} \left(4112 \cdot a_B \cdot R_B\right) & \text{if } a_B < 0.34 \\ \left[\left(1349 + 110 \cdot a_B\right) \cdot R_B\right] & \text{if } a_B \geq 0.34 \end{cases}$$

$P_B = 1968$ (kips)

REFERENCES

American Association of State Highway and Transportation Officials (AASHTO). Guide Specification and Commentary for Vessel Collision Design of Highway Bridges. American Association of State Highway and Transportation Officials, Washington, DC, 1991.

American Association of State Highway and Transportation Officials (AASHTO) LRFD Bridge Design Specifications and Commentary. Washington, DC: American Association of State Highway and Transportation Officials, 1994.

Bullock P., Wasman S., McVay M., Subsurface Investigation and Monitoring of Vessel Impact Testing at the St. George Island Bridge, Florida, Transportation Research Record: Journal of the Transportation Research Board, In press.

Consolazio, G.R., Cook, R.A., Lehr, G.B., Bollmann, H.T., Barge Impact Testing of the St. George Island Causeway Bridge Phase I: Feasibility Study, Structures Research Report No. 783, Engineering and Industrial Experiment Station, University of Florida, Gainesville, Florida, January 2002.

Consolazio, G.R., Cook, R.A., Biggs A.E., Cowan, D.R., Bollmann, H.T., Barge Impact Testing of the St. George Island Causeway Bridge Phase II: Design of Instrumentation systems, Structures Research Report No. 883, Engineering and Industrial Experiment Station, University of Florida, Gainesville, Florida, April 2003.

Consolazio, G.R., Cowan, D.R., Biggs, A.E., Cook, R.A., Ansley, M., Bollmann, H.T., Full-scale Experimental Measurement of Barge Impact Loads on Bridge Piers, Transportation Research Record: Journal of the Transportation Research Board, In press.

El Naggar M. H., Bentley K.J., Dynamic Analysis for Laterally Loaded Piles and Dynamic p-y Curves, Can. Geotech. J. 37, pp. 1166-1183, 2000.

ENSOFT, Inc., GROUP 5.0 Technical Manual, Austin, Texas, 2000.

Florida Bridge Software Institute, FB-Multipier User's Manual, University of Florida, Gainesville, FL, 2005.

Knott, M., Prucz, Z., Vessel Collision Design of Bridges: Bridge Engineering Handbook, CRC Press LLC, Boca Raton, FL, 2000.

Livermore Software Technology Corporation (LSTC). LS-DYNA Keyword User's Manual. Livermore, CA, 2003.

McVay, M.C., O'Brien, M., Townsend, F.C., Bloomquist, D.G., and Caliendo, J.A. Numerical Analysis of Vertically Loaded Pile Groups, ASCE, Foundation Engineering Congress, Northwestern University, Illinois, pp. 675-690, July, 1989

Mokwa, R.L. Investigation of the Resistance of Pile Caps to Lateral Loading, Ph.D. Dissertation, Virginia Polytechnic Institute and State University, Blacksburg, Virginia, 1999.

National Transportation Safety Board (NTSB), U.S. Towboat Robert Y. Love Allision With Interstate 40 Highway Bridge Near Webbers Falls, Oklahoma May 26, 2002, Highway-Marine Accident Report NTSB/HAR-04/05 Washington, DC: NTSB, 2004.

Saul, R., and Svensson, H. Means of Reducing the Consequences of Ship Collisions with Bridges and Offshore Structures. Proc., Int. Assn. For Bridges and Struct. Engrg. (IABSE) Colloquim, Ship Collision with Bridges, Introductory Rep., IABSE-AIPC-IVBH, Copenhagen, 165-179 (1983).

US. Army Corps of Engineers, Engineering and Design Barge Impact Analysis for rigid walls, Technical letter No. 1110-2-563, Sept. 30, 2004.

BIOGRAPHICAL SKETCH

The author was born in Hanoi, Vietnam. He began attending the Hanoi University of Civil Engineering in September 1994, and received a Bachelor of Science in civil engineering in June 1999. After his undergraduate studies, he worked as a project engineer at VINACONEX Construction Corp. in Hanoi, Vietnam. In 2003, he received a full scholarship from the Vietnamese government for master's study and began graduate school in the College of Engineering at the University of Florida to pursue a Master of Engineering degree. The author plans to complete his Master of Engineering degree in August 2005 and join the PhD program at the University of Florida.